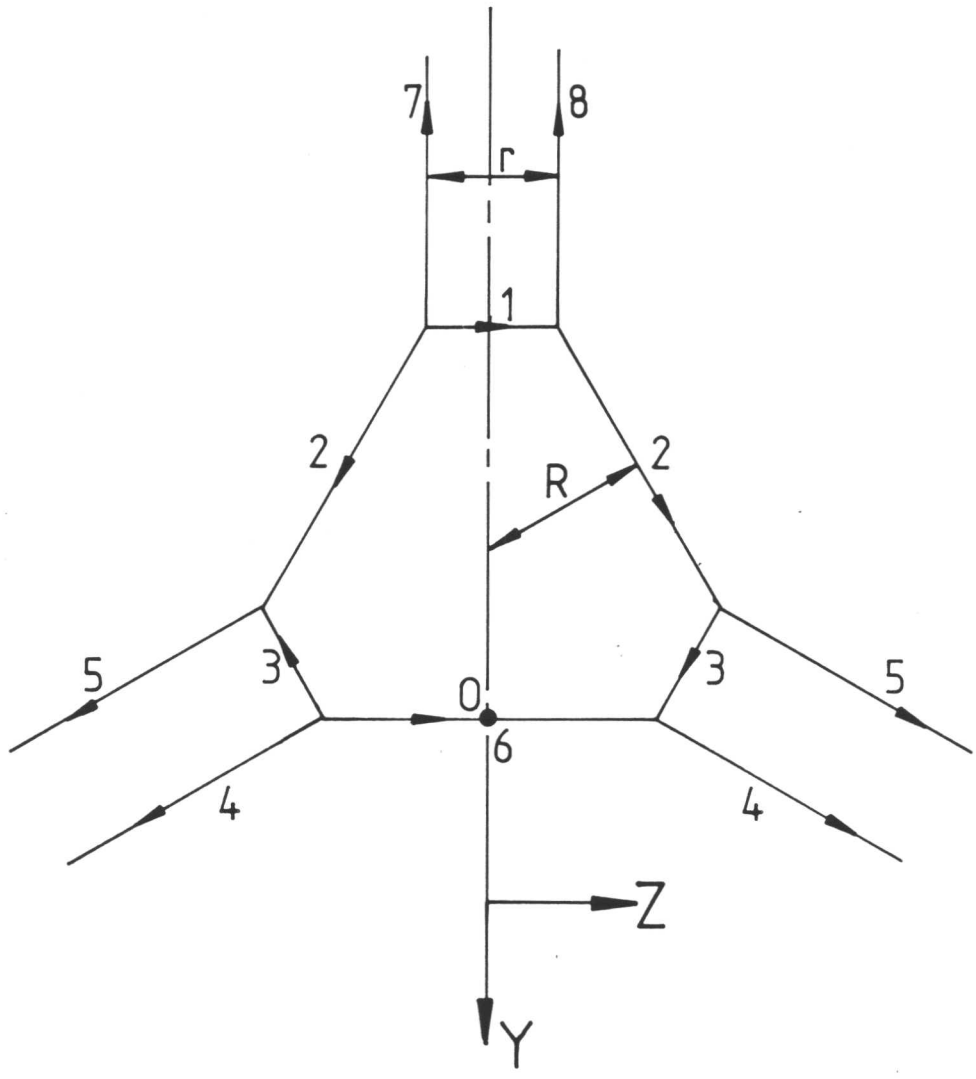

Fig. 6.6. Supernode dislocation configuration used to evaluate SSF energy. Only five dislocation stresses are required because the supernode is symmetrical. Dislocations 7 and 8 have no component in the Z direction and can therefore be ignored. See appendix D for details.

for pure screw dislocations, a is the gamma prime lattice parameter, R is the internal dimension of the node, and G(ρ) is the geometrical function.

If G(ρ) is plotted as a function of ρ (fig. 6.7) it is found that when ρ is zero G=3.82 and lies within 8% of that value until ρ=1.3. Between ρ=1.3 and $\sqrt{3}$ the SSF energy rapidly increases to infinity since the strain field of dislocation 6 is decreasing as its length decreases, and the strain fields of the infinitely long dislocations 4 and 5 become dominant. When ρ≤1.3 the SSF energy is relatively insensitive to ρ and therefore the superdislocation spacing, r. In this region the SSF energy can be approximated to equation 6.9:

$$\gamma_{SSF} = \frac{K}{R} \qquad \text{eqn. 6.9}$$

in this case $K=0.654Jm^{-2}$.

As the length of the $a/_3<211>$ dislocations becomes shorter the centre of the node becomes more like a triangle and the SSF energy rises very rapidly. In this configuration (fig. 6.8a) the Rae-Hillier model predicts that an energy of many Joules would be necessary to maintain the shape. It is proposed that when $r>\sqrt{3}R$ the configuration shown in figure 6.8(b) may form. In this investigation the unextended nodes adopted the configuration shown in figure 4.19(d). The configuration shown in figure 6.8(b) will not be discussed further.

6.3.2 SSF energy measurement

In 6.3.1 it was shown that the SSF energy is a function of ρ. Rae and Hillier (1984) have computed the superlattice stacking fault energy, γ_{SSF}, from the true superdislocation spacing, r, and the internal dimension of the node, R. Values of r and R were measured from weak beam dark field electron micrographs of foils with approximately <111> normals. In all cases it was assumed that the nodes were planar and that the dislocations adopted the equilibrium spacing on that plane. This was seen to be true even when the superdislocations at the nodes were twisted between the

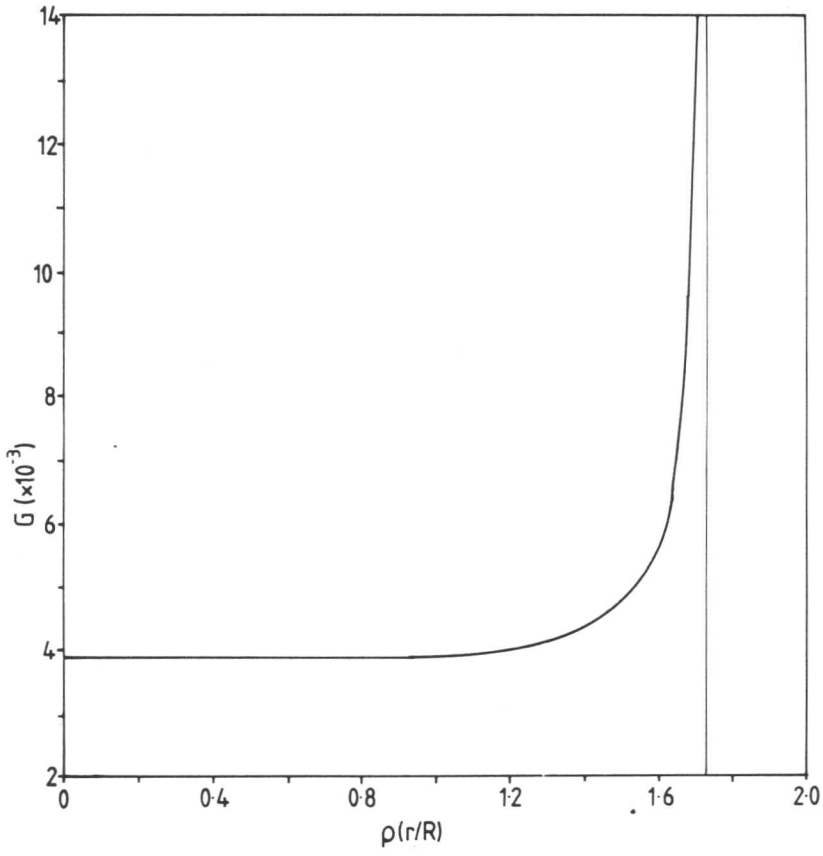

Fig. 6.7. Dependence of the geometrical function, $G(\rho)$, on ρ.

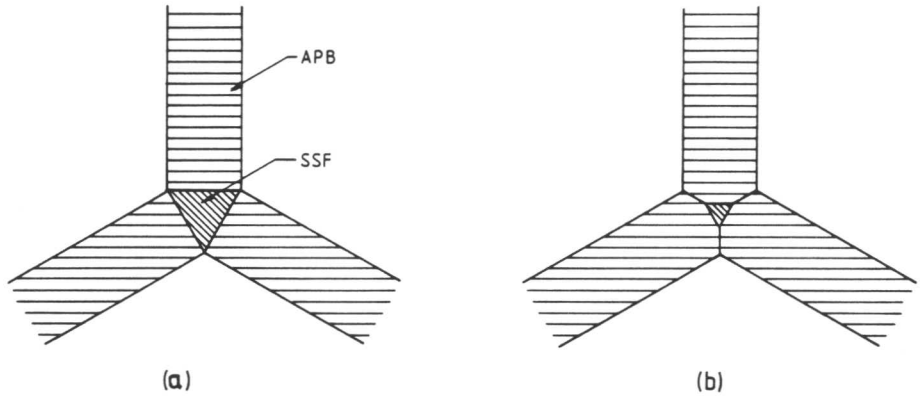

Fig. 6.8. Illustration of the supernode configuration with an infinite SSF energy (a) and the configuration which may replace it at high SSF energies (b).

SSF plane and the APB plane. The values measured were corrected for foil tilt before the fault energies presented in 6.3.3 were computed.

6.3.3 Results

The superlattice stacking fault energies are shown graphically in figure 6.9. The dislocation spacings at the node, r, the internal dimension, R, the ratio r/R, ρ, and the energies, γ_{SSF}, are listed in full in appendix F. The results are summarised in table 6.2 and the total number of node observations are shown in table 6.3.

The trends can be seen most clearly in figure 6.9. The SESF energy is always lower than the SISF energy, as expected from the relative node size. Both energies decrease as the titanium content of the alloy is increased. The SESF decreases more sharply than the SISF. The standard deviation and range of the SSF energies is considerably smaller than those for the corresponding APB energies. It is thought that this is because the SSFs are stabilised by a diffusion process at the annealing temperature and unlike the APBs are unable to contract during cooling from the annealing temperature. It is thought that the SSF energy values are typical of 1173K, the annealing temperature.

The SISF energies measured from alloys A and D could be significantly in error because the values of ρ are greater than 1.3 for these alloys. (See appendix F.) Rae and Hillier (1984) have shown that under these conditions the SSF energy is very sensitive to small changes in superdislocation spacing; the value can change by $60mJm^{-2}$ for a 1nm change in r. As a consequence of this, any error in the measurement of r and R could have a significant effect on the SISF energy values. Also, most of the supernodes containing SISFs in alloy G were not extended and the SISF energy could not be measured from them.

In summary, as shown in figure 6.9, at 1173K the SESF energy is considerably lower than SISF energy. The SESF energy decreases at a

Table 6.2. Summary of Superlattice Stacking Fault Energies

	Alloy		
	G	D	A
γ' Ti content (at.%)	2.8	3.3	3.9
Mean extrinsic SSF energy (mJm^{-2})	94	74	46
Standard deviation (mJm^{-2})	10	5	5
Mean intrinsic SSF energy (mJm^{-2})	137	131	117
Standard deviation (mJm^{-2})	-	7	1

Table 6.3. Number of Node Observations

Alloy	Node Type				Total Observations
	Extended Extrinsic	Not extended Extrinsic	Extended Intrinsic	Not extended Intrinsic	
A	8	1	7	1	17
D	9	0	6	3	18
G	5	2	1	6	14

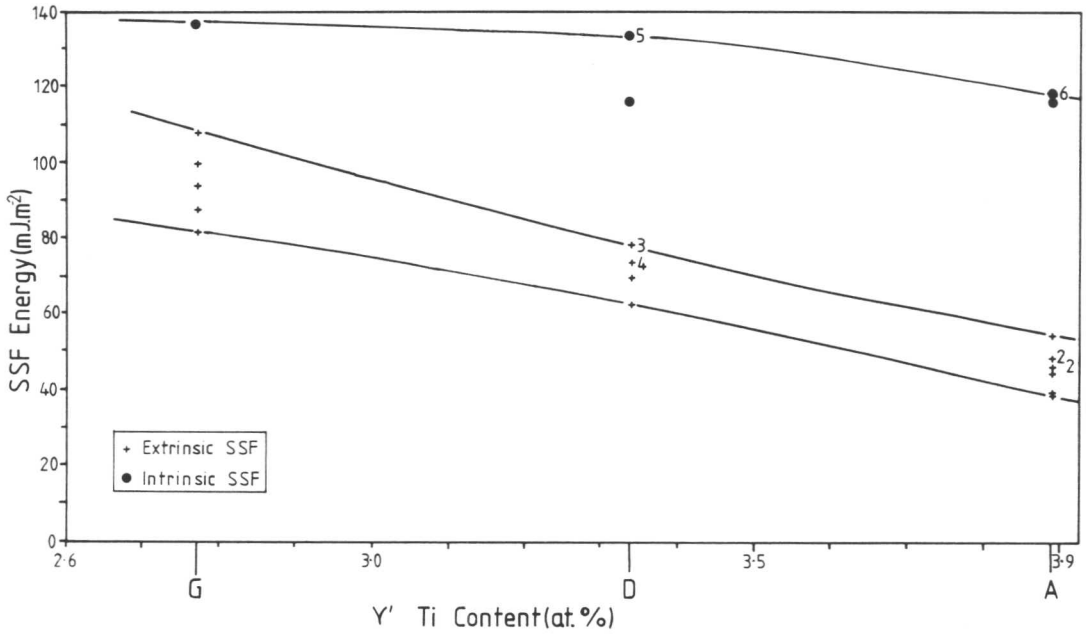

Fig. 6.9. The variation in the SSF energies with γ' titanium content for alloys A, D and G. Numbers next to points indicate the number of measurements represented at that point.

higher rate than SISF energy. The SESF energy drops by approximately 50% with a 1.1 at.% change in the γ' titanium content while the SISF energy falls by only 14% for the same change. The values exhibit a smaller scatter than the APB energies because it is thought that they are stabilised at the annealing temperature.

6.3.4 Discussion

The author is aware of only three values of SSF energy in $L1_2$ structures which have been published prior to this investigation. The first by Leverant and Kear (1970) is a value for the SISF energy in the gamma prime measured from a creep specimen of Mar-M 200. The value quoted is 8-17mJm^{-2}. Leverant and Kear do not state how they arrived at this figure. It is thought that they measured the spacing between the dislocations bounding a SISF forming part of a superdislocation shearing the gamma prime. The value is very small, perhaps because no account was taken of the influence of surrounding dislocations and faults. The dislocation and fault arrangement at these defects has been shown to be complex (Kear et al. 1969 and Rae, 1984), and any calculation of fault energies from them is expected to be extremely complicated. As this value was measured from a crept specimen where the faults may not be in equilibrium, and no information has been given by the authors to explain how they evaluated the quoted value, it was treated with suspicion.

The other values were measured from other $L1_2$ structures. Sastry and Ramaswami (1976) have measured the APB energy and an unspecified SSF energy thought to be the SISF energy at room temperature in Cu_3Au. From dislocation spacings they concluded that the SISF energy was considerably lower than the APB energy. Howe et al. (1974) measured what they claim to be the SISF energy of Zr_3Al using a dislocation spacing method similar to that used to measure the APB energy in this investigation. They found the energy to be between 70 and 90mJm^{-2} and confirmed their results by measur-

ing the SISF energy of nodes using the method described by Brown and Thölen (1964). It seems, however, (see 4.6) that Howe et al. incorrectly identified the dislocation pairs they observed and their interpretation of the network dislocation structure is doubtful. It has been shown that due to the difference in structure between dislocation networks in ordered and disordered materials it is incorrect to apply the method of Brown and Thölen to superdislocation networks in $L1_2$ structures. It is suggested that the energy values quoted by Howe et al. are not SSF energies. An important observation made by Howe et al. which will be considered later was that the SISFs and SESFs were extended by about the same amount.

Although so few SSF energy values have been measured, Kear et al. (1968) pointed out that the stacking sequence at an SISF was equivalent to four layers of the DO_{24} (Ni_3Ti) structure or four layers of the DO_{19} structure while the stacking sequence at an SESF was equivalent to seven layers of the DO_{24} structure. They also pointed out that these SSFs could be stabilised by segregation of DO_{24} forming elements such as titanium. This stabilisation process has also been proposed by Leverant and Kear (1970) and Kear et al. (1970).

By using a novel approach, values for the SSF energies of the gamma prime in three superalloys with different titanium contents have been evaluated and show that the SSF energy drops with increasing titanium content. These observations strongly suggest that the predictions of Kear et al. (1968) are correct and that titanium does segregate to the nodes and stabilise the nodes by forming a titanium rich region or perhaps precipitating very thin planar Ni_3Ti. Such precipitation has previously been observed on stacking fault in the titanium rich superalloy Nimonic 901 by Oblak et al. (1971) and in Udimet 700 by Kear et al. (1970).

In this investigation the extrinsic SSFs were seen to be more extended than the intrinsic SSFs; this is expected as the SESF has a

greater thickness of DO_{24} than the SISF implying that it is likely to be stabilised by a greater degree. Also similar extended nodes observed in Zr_3Al by Howe et al. (1974) which contained no DO_{24} stabilising elements were seen to be equally extended - another observation supporting titanium segregation to the SSFs.

The stabilisation of SSFs by the precipitation of Ni_3Ti is a diffusion controlled process. It is expected that the apparent SSF energy of the stabilised faults will decrease with time until an equilibrium related to the overall titanium content of the alloy is reached. This is borne out in the SSF energy values measured. It can be seen from figure 6.9 that the alloy containing the smallest amount of Ti has the highest SSF energies.

The titanium which stabilises the fault can migrate from either the gamma matrix or the gamma prime itself, and it can arrive at the fault either by bulk diffusion through the γ' or by diffusion through γ and/or γ' to dislocation cores followed by rapid diffusion along the dislocation cores.

Very few data are available for Ti diffusion in γ'. The best available value is that reported by Larikov, Geichenko and Fal'chenko (1981) in $Ni_3(Al_{0.6}Ti_{0.4})$. They report that at 1223K the activation energy for the bulk diffusion of Ti in $Ni_3(Al_{0.6}Ti_{0.4})$ was $145 kJmole^{-1}$ and the pre-exponential factor, D_o, was $1.9 \times 10^{-10} m^2 s^{-1}$. The simple diffusion equation $X=\sqrt{Dt}$ was applied for a γ' particle size of 0.5μm and this showed that bulk diffusion of Ti to a fault in the centre of a γ' particle would occur in about 16 minutes at the annealing temperature of 1173K. The γ' precipitates in alloys A, D and G are compositionally more complex than the alloy studied by Larikov et al. They contain elements such as tantalum and tungsten which are expected to lower diffusion rates. Consequently, titanium diffusion will be slower so fault stabilisation will take considerably longer in these alloys.

However, this simple approach does show that it is quite plausible for titanium to diffuse to, and stabilise, the SSFs.

Many more diffusion data are required before a quantitative assessment of titanium diffusion and fault stabilisation in single crystal superalloys can be made.

In summary, there is strong evidence to suggest that Ti stabilises SSFs by forming thin planar regions of Ni_3Ti on the fault planes. Consequently, the SESF energy is lower than the SISF because the SESF is equivalent to a larger portion of the Ni_3Ti lattice than the SISF. There is also evidence to suggest that the stabilisation is greater in alloy A than in alloy G because A contains more Ti. Tables 2.1 and 2.2 show that the γ matrix of alloy A contains twice as much Ti as the γ of alloy G while there was about 40% difference in the γ' Ti contents. It is suggested that stabilisation of SSFs by the precipitation of Ni_3Ti on the favourable sites at the nodal points occurred by bulk diffusion of Ti through γ and γ' to faults and to dislocations which then provide rapid transport to faults. The rate controlling step will be the bulk diffusion of Ti in γ and γ' either to the faults or to the dislocation cores.

The SSF energies shown in figure 6.9 and table 6.2 are the values at the annealing temperature of 1173K. It would be interesting to examine extended nodes at other temperatures to study the effect of temperature on SSF energies. Another useful experiment would be to follow diffusion of Ti and other alloying elements by a radioactive tracer to evaluate the diffusion coefficient and prove that fault stabilisation is occurring.

The stabilisation of SSFs and the difference in the energies between APB and SSF could be important to the mechanical properties of superalloy materials. This aspect of alloy behaviour is discussed in the next chapter.

6.4 Conclusions

(i) It is found that the APB energy calculated from measured dislocation spacings is not sensitive to alloy titanium content for γ' titanium between about 2.7 and 3.9at.%.

(ii) The mean APB energy is $83\pm20 mJm^{-2}$.

(iii) The first analysis of supernodes has allowed the evaluation of SSF energies from supernode geometry. This technique, proposed by Rae and Hillier, can be used to study the SSF energies of other superalloy materials.

(iv) It is found that SISF and SESF energies decrease as alloy Ti content increases as shown in figure 6.9.

(v) The SESF energies were found to be 94 ± 15, 74 ± 10 and $46\pm12 mJm^{-2}$ for alloys G, D and A respectively, and the equivalent SISF energies were 137, 131 ± 10 and $117\pm5 mJm^{-2}$ respectively.

(vi) It is suggested that diffusion of Ti to the nodal points by diffusion through the γ,γ' and along dislocation cores stabilises the SSFs by forming thin planar regions of Ni_3Ti.

(vii) The SESF energy is considerably lower than the SISF energy because the SESF is equivalent to a greater number of planes of Ni_3Ti stacking.

CHAPTER 7

THE EFFECT OF TITANIUM ON DEFORMATION MECHANISMS IN SINGLE CRYSTAL SUPERALLOYS

7.1 Introduction

The important variables influencing the strength of Ni-base superalloys are (see 1.5.3):

(i) Solid solution strengthening of the γ

(ii) The γ' volume fraction

(iii) The γ' particle size

(iv) Misfit strengthening

(v) The superlattice stacking fault and antiphase boundary energies.

The inaccurate determination of these parameters and the failure to consider their interdependence create uncertainties in the various deformation models proposed. This chapter reviews the established deformation model and proposes a modification to that model as a result of the energy data reported previously. The modified model is then used to explain the stress-rupture results reported in chapter 1.

It is well documented that different heat treatments can affect alloy properties by producing differences in precipitate size and distribution (e.g. Decker, 1969). It is also reported that changes in alloy composition can affect precipitate volume fraction (Decker, 1969) and γ/γ' misfit (e.g. Grouse and Ansell, 1981). For the purposes of this investigation it was necessary to keep factors (i) to (iv) constant so that the only variable parameters were the APB and SSF energies. Any changes can then be attributed to variations in the alloy Ti content (as proposed by Roome, 1982).

Factors (i) to (iii) were kept constant by choosing a small compositional range, near to the value of interest and using a long homogenisation treatment so that changes due to compositional variations were negligible. The mean precipitate size of each alloy was the same because each specimen underwent an identical heat treatment cycle. Factor (iv) was also seen to be constant as there was no observable γ/γ' misfit in any of the alloys (see 2.9). Hence, the only variable quantities were the SSF and APB energies. Any observed change in stress rupture life between the alloys must have been due to the change in fault energies brought about by the change in titanium content.

7.2 Deformation Modes in Ni-Base Superalloys

Pope and Ezz (1984) have recently produced a comprehensive review of the established deformation mechanisms and the mechanical properties of high volume fraction γ' superalloys. The present work therefore focuses on deformation mechanisms involving dislocation glide through the γ' and the effect changes in titanium may have upon these mechanisms are discussed. It is emphasised that much of the material's strength is derived from the ability of the γ/γ' interface to resist the passage of dislocations into the γ'. This is borne out by the observation that single-phase polycrystalline γ' alloys creep much more rapidly than two-phase γ/γ' alloys (Pope and Ezz, 1984).

7.2.1 Information from the deformation-mechanism map

As far as the author is aware only one creep deformation-mechanism map has been produced for a large grain size high volume fraction γ' superalloy. A reproduction of this map, for Mar-M 200 (Frost and Ashby, 1982), is shown in figure 7.1. The test conditions used to generate figure 1.1 are shown on the map and it can be seen that these three conditions lie either in the power-law creep or plasticity regions. Power-law creep is a region where deformation is usually dominated by dislocation glide and

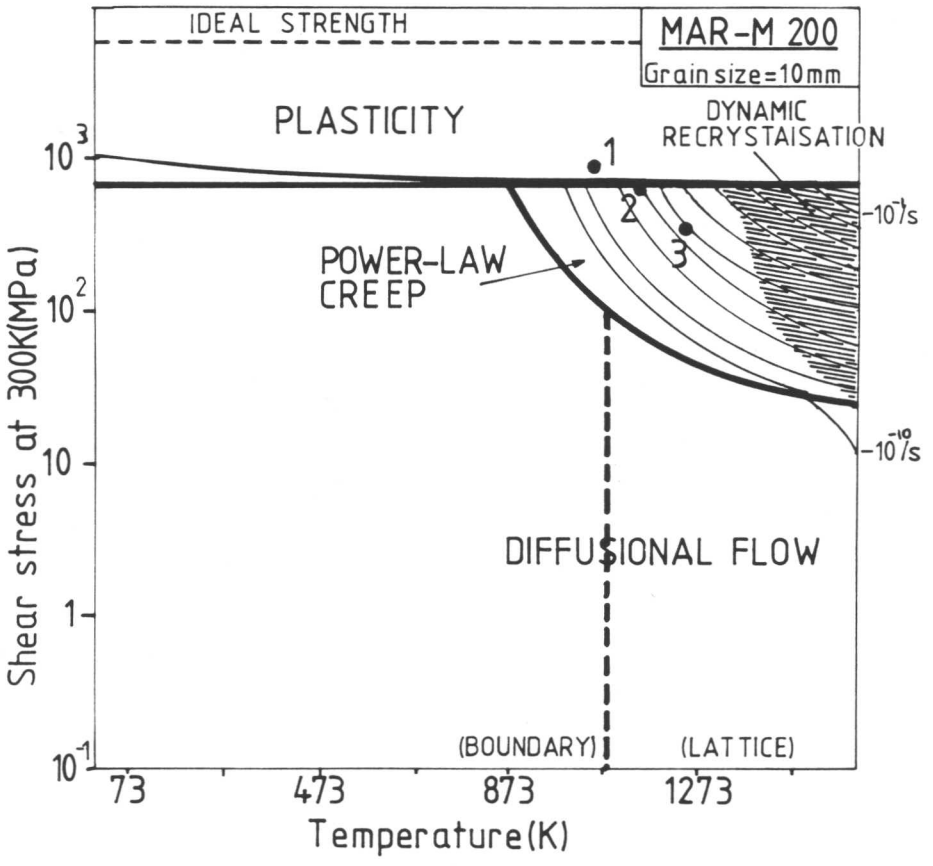

Fig. 7.1. Deformation mechanism map for Mar-M 200 (table 1.1) with a grain size of 10mm from Frost and Ashby (1982). The test conditions used in this investigation are marked on the map: 710MPa at 1023K (1), 430MPa at 1123K (2) and 225MPa at 1223K.

climb while plasticity is dominated by glide alone. The deformation map is, however, not for a single crystal and admitted, by its authors, to be approximate, therefore, the information drawn from it is not definitive but it seems that deformation will be controlled by dislocation glide and climb.

7.2.2 Deformation by dislocations looping around the γ'

The majority of mechanisms proposed to explain the strengthening of Ni-base superalloys appear to have been based on the assumption that deformation will only occur by the glide of dislocations through the γ' because the particles are so close together that the dislocations would have to follow such a tortuous route that looping and climb would not occur. Only one deformation mechanism proposed to explain the strengthening of high volume fraction γ' alloys considers looping or climb to be an important mechanism. This is due to Carry and Strudel (1975, 1977, 1978) and Carry, Houis and Strudel (1981) who state that deformation occurs by the glide of $a/_2\langle 110\rangle$ dislocations on $\{110\}$ planes in the γ to form networks in the γ/γ' interfaces. At high temperatures it is proposed that these dislocations climb over the γ' particles rather than gliding through them.

No analysis of the slip planes of $a/_2\langle 110\rangle$ dislocations in the γ was undertaken in this investigation but it is thought rather unlikely that slip would occur on the non-close packed $\{110\}$ planes suggested by Carry and Strudel. The movement of dislocations within gamma and the structure at the γ/γ' interfaces have been largely ignored by researchers studying superalloy deformation in high volume fraction γ' superalloys. It is suggested earlier (4.4.2) that the regions of γ between the precipitates are so small that at low temperatures it is unlikely that many superdislocations can be formed easily. Unpaired dislocations will have little chance of entering the γ' so for deformation to occur they must loop around the particles. This is known to occur in lower volume fraction γ' alloys,

see for instance Davies and Stoloff (1965).

Many fewer dislocations were observed in the γ' than the γ and this suggests that up to about 1000K a significant number of dislocations by-pass the γ' precipitates. It appears that dislocation looping and climb may be a significant strengthening mechanism during power-law creep and the dislocation behaviour in γ would be worth investigating.

7.2.3 Deformation by dislocations gliding through the γ'

Glide of dislocations through γ' frequently occurs and it is thought that much of the improvement in superalloy properties in recent years has been due to the steady increase in resistance to γ' glide produced by careful alloying.

(i) Shearing by superdislocations

The most common γ' shearing mode is the passage of superdislocation, consisting of pairs of $a/_2\langle 110\rangle$ dislocations on {111} planes bounding an APB (fig. 7.2 and Kear and Oblak, 1974). Superdislocation shear is the dominant γ' shearing mode up to about 1000K in creep and up to about 1100K in tensile deformation. In creep, between 1000K and 1200K the dominant shearing mode is partial dislocation shear.

At temperatures above ~1200K shear by superdislocations becomes dominant again (Leverant et al., 1973). Leverant et al. proposed that this change was due to a precipitous drop in the APB energy caused by rapid diffusion at the dislocation core leading to local lowering of the order. This proposal seems a highly unlikely explanation for the change in deformation mode observed at high temperatures.

(ii) Shearing by partial dislocations

In the temperature range between 1000K and 1200K shear of γ' occurs by the passage of partial dislocations (Kear et al., 1969 and Leverant and Kear, 1970). This has been shown to occur either by the passage of $a/_3\langle 211\rangle$ partial dislocations producing single SSF ribbons (fig. 7.3a), which are

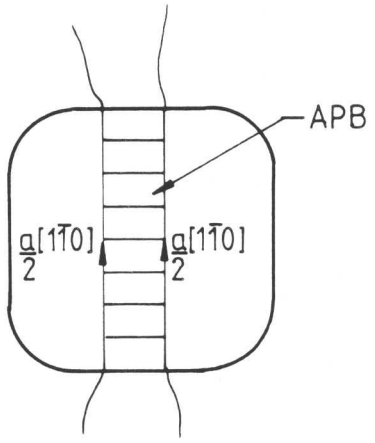

Fig. 7.2. γ' shearing by a superdislocation of two $a/_6[110]$ dislocations.

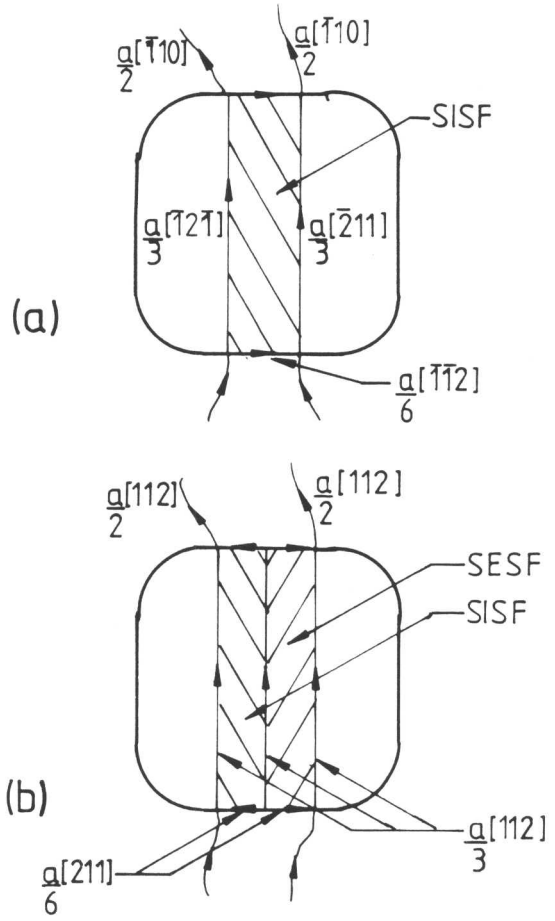

Fig. 7.3. γ' shearing by a pair of $a/_3\langle 211\rangle$ partial dislocations bounding a SSF (a), and a triplet of $a/_3\langle 211\rangle$ partial dislocations forming a SISF/SESF pair. In both instances an $a/_6\langle 211\rangle$ partial dislocation is required in the γ/γ' interface

produced by a superdislocation of two identical $a/_2$<110> dislocations in the γ, or by SISF/SESF fault pairs (fig. 7.3b), which are produced by groups of dislocations in the γ with a complete Burgers vector of a<211>. Although the SISF/SESF pair deformation mechanism appears rather unlikely they have been observed by Kear et al. (1969), Roome (1982) and Rae (1984); also Leverant and Kear (1970) showed that the rotations of the tensile axes of creep specimens were consistent with the <112> {111} slip mode.

As shown in figure 7.3, both these mechanisms require the production of various partial dislocations at the γ/γ' interface. Leverant and Kear (1970) suggest that the dislocation dissociations required to form SISF/SESF pairs will not occur at lower temperatures because they require thermal activation to nucleate an additional dipolar dislocation at the dislocation core. A more likely mechanism is that due to Rae (1984) who proposes that the 'dipole displacement' is unnecessary because two different $a/_2$<110> dislocations may combine at intermediate temperatures to produce $a/_2$<211> dislocations which can subsequently dissociate to produce the $a/_3$<211> dislocations required to form SISF/SESF pairs.

(iii) Other mechanisms

Many mechanisms which enhance the strengthening effect of the main shear modes by the creation of dislocation jogs and loops have been reported. Some of these are described in 5.2.2 and 5.2.3 and discussed with the debris hardening mechanism proposed by Thornton et al. (1970) and the cross-slip mechanism of Takeuchi and Kuramoto (1973) in 5.4. These mechanisms also help to increase the alloy properties by enhancing resistance to γ' shear.

7.2.4 Established model for γ' shear during creep

Kear et al. (1968) first suggested that at any given temperature the most prolific shearing mode will be that which has the lowest fault energy. On this basis it was suggested that the change in shear mode observed between 1000K and 1200K occurred because the SSF energy falls below

the APB energy; both energies were assumed to decrease with increasing temperature. It was also observed that the required dislocation dissociations into $a/3\langle 211\rangle$ partial dislocations were more likely at higher temperatures (Leverant and Kear, 1970, and Rae, 1984).

At temperatures above 1200K it was predicted that the APB energy decreased rapidly due to local disordering at the dislocations (Leverant et al., 1973) and deformation was again seen to occur by superdislocation glide. These ideas are summarised schematically in figure 7.4(a).

7.3 Modified Model for γ' Shear During Creep

In 5.4 and 6.3 evidence was presented to indicate that the diffusion of Ti to SSFs stabilised the faults by forming very thin planar Ni_3Ti on the fault plane. This stabilisation process could have a significant effect on γ' shearing and it was with this in mind that the modified deformation mechanism presented below was produced.

The refined model is based on an extension of Kear's hypothesis that the most prolific slip mode will be the one with the lowest fault energy. It is noted that in addition to the fault energy the dislocation Burgers vector, the applied stress and the dislocation friction stress will also contribute to the overall deformation mechanism. The fault energy, however, is considered to be the most important factor because under the conditions used in this investigation the applied stress is constant and the magnitudes of the dislocation Burgers vectors of $a/2\langle 110\rangle$ and $a/3\langle 211\rangle$ dislocations differ by only 12%.

Between room temperature and about 1000K γ' shearing occurs by the glide of pairs of $a/2\langle 110\rangle$ dislocation on $\{111\}$ planes. At low temperatures little γ' shear occurs because only a few superdislocations can form (4.4.2): the majority of the deformation occurs by dislocation looping. As the temperature is increased the APB energy steadily decreases due to an increase in entropy producing a small reduction in the long range order parameter. This would be manifested by a small increase in the super-

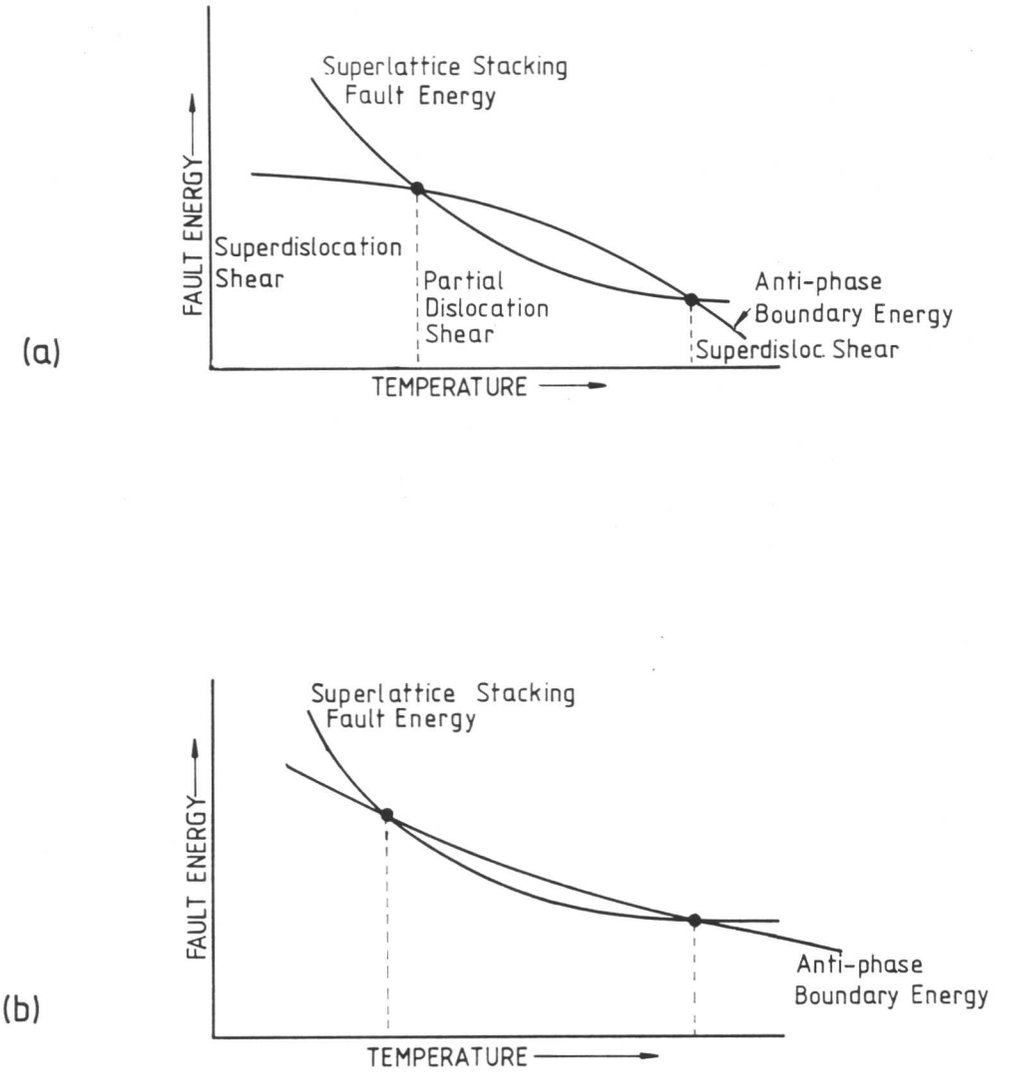

Fig. 7.4. Schematic plot of the APB and SSF energies vs. temperature for the model proposed by Leverant and Kear (1970) (a), and that proposed in this investigation (b).

dislocation spacing.

It is proposed that at a temperature just below 1000K the Ti diffusion rate is sufficiently fast to stabilise SISFs and SESFs and there is enough thermal energy available for unpaired $a/_2<110>$ dislocations to combine in the γ to form $a/_2<211>$ dislocations which subsequently dissociate into $a/_3<211>$ partial dislocations. When the energy of this dislocation combination falls below that of an APB bounded by two $a/_2<110>$ dislocations partial dislocation shear will occur. In addition this mechanism reduces the number of $a/_2<110>$ dislocations able to form superdislocation pairs, thus reducing the frequency of superdislocation shear.

It is suggested that free titanium, either in the γ or the γ', diffuses towards the newly formed SSF through the precipitate, the matrix and along the dislocation cores. The SSF is stabilised by the agglomeration of titanium on the fault plane or by the formation of a thin planar precipitate of Ni_3Ti. This process will lower the energy of the SSF and allow it to extend further into the γ'. The stabilisation of superlattice stacking faults in this way can be likened to Suzuki locking seen in non-ordered materials (Suzuki, 1952; as discussed by Nabarro, 1967). The SSF will expand until the equilibrium spacing equivalent to the stabilised fault energy is reached. At this point the fault may stretch across more than one γ' particle. The stabilisation process will have no effect on the dislocation configuration during deformation. It will only act to delay the passage of those dislocations through the gamma prime.

Once segregation has occurred the dislocation configuration will only be able to continue its motion through the γ' particle by diffusion of Ti with the fault or by the dissolution of the stabilising atmospheres at high temperatures where the increase in entropy means that the system energy cannot be lowered by segregation to the SSFs. Consequently, as temperature increases, the retarding of gliding partial dislocations by Ti segregation will become increasingly unlikely, perhaps leading to an apparent increase

in SSF energy. Consequently the mechanism will only be effective over the temperature range when the diffusion rate of the pinning species is fast enough to allow Ti to migrate with the dislocations, to the temperature when the thermal energy is so great that the pinning species cannot lower its energy by migrating to the fault.

A simple calculation has been made using an estimated dislocation density, an approximate creep rate and the diffusion data of Larikov et al. (1981) for $Ni_3(Al_{0.6}Ti_{0.4})$ (appendix G). This shows that diffusion would occur rapidly enough to allow Ti to move with the dislocations and stabilise an SSF at temperatures above 630K. However, the γ' precipitate in alloys A, D and G is more highly alloyed than $Ni_3(Al_{0.6}Ti_{0.4})$. It contains W which was seen to lower the diffusivity of Ti in Ni at 1170K (Pridantsev, 1967) and Ta which is expected to have a similar effect. Consequently it is suggested that the diffusivity of Ti may be reduced in complex superalloys and that fault stabilisation will not occur at temperatures as low as 630K. Little is known of the diffusion constants of Ti in modern superalloys, and much further work is required to evaluate accurate diffusion coefficients and dislocation velocities in these materials before accurate values for the temperature at which Ti stabilises moving faults can be determined. It does, however, appear that fault stabilisation is possible. It must be remembered that γ' shearing by partial dislocations will not occur during creep deformation regardless of whether SSF stabilisation is possible until the total energy for the process is lower than the total energy for superdislocation shear.

At higher temperatures dislocation pinning does not occur. It was observed that superdislocation shear becomes dominant again. This is probably not due to any precipitous drop in the APB energy but rather to a combination of the decrease in SSF stabilisation and the increased climb of dislocations in the γ matrix. Unpaired $a/_2\langle 110\rangle$ dislocations will climb until two like dislocations inhabit the same {111} plane. It will then be

favourable for the newly formed superdislocations to glide through the γ'. This mechanism involving the decrease in SSF stabilisation and the increase in dislocation climb appears to be more likely than the local disordering mechanism suggested by Leverant et al. (1973) which was reported earlier. Figure 7.4(b) is a schematic diagram showing how the variations in fault energy with Ti content differ from those assumed before (fig. 7.4a).

No TEM investigation was undertaken to verify this modified deformation because it was felt that this would be of little value, as the proposed change is a reinterpretation of previous results.

7.4 The Effect of Titanium on Stress-Rupture Life

Stress-rupture tests designed by the author were kindly undertaken by Rolls-Royce Ltd., Derby to assess the effect of Ti variation on the stress-rupture life of alloys A, D and G. These results were referred to in chapter 1 (fig. 1.13). They are the only results which have been performed on a set of alloys with systematic variations in Ti which had undergone identical heat treatment cycles. After homogenisation for 36 hrs at 1573K followed by a slow argon gas fan quench to room temperature and a subsequent 16 hr ageing treatment at 1143K, the specimens were machined to a standard Rolls-Royce test piece. This heat treatment was used to produce a microstructure which was as close as possible to that used for fault energy measurement (2.4). Before testing, the specimen orientations were measured using the Laue back reflection X-ray technique. All the specimens except three had their initial tensile stress axis within 8° of [001], the others were between 8° and 14° of [001]. There were no obvious differences in deformation behaviour. Consequently, specimen orientation effects were ignored.

The specimens were tested at 710MPa/1023K, 430MPa/1123K and 225MPa/1223K. The results are listed in appendix A and plotted in figure 1.13. It is clear that small increases in the Ti content considerably improve the

stress-rupture life at 1023K and 1123K. At 1223K the improvement in properties still occurs but is less substantial.

The γ' shearing mode at 1023K and 1123K is expected to be a combination of superdislocation and partial dislocation shear. The effects of this are discussed in 7.5. At 1223K it is expected that γ' shearing would be occurring mainly by $a/_2\langle 110\rangle$ {111} superdislocation glide with only a small contribution from partial dislocation glide; however, some of the deformation would be occurring by the climb of $a/_2\langle 110\rangle$ dislocations in the γ matrix allowing dislocations to by-pass the γ' particles.

7.5 The Effect of SSF and APB Energies on Stress-Rupture Life

The fault energy measurements reported in chapter 6 were representative of a temperature at or a little below 1173K. They should therefore show the best correspondence with the tests conducted at 1123K. The following discussion relates the measured energies at 1173K with the stress-rupture properties at 1123K.

It is clear from figure 1.17 that there is a major increase in stress-rupture life between alloy D and alloy A. This is in agreement with the observations of Roome (1982) who noted a drastic improvement in properties with a difference of 0.8at.% Ti from 1.84at.% to 2.62at.% Ti in overall alloy Ti content.

It is proposed that the improvement in stress-rupture life is brought about by a change in deformation mechanism due to the change in total fault energy induced by Ti. If it is assumed that the unstabilised SSF energies are equal for all three alloys, the APB energy would be considerably lower than the SSF energies, and deformation would occur only by superdislocation shear because it has the lowest total configuration energy. However, it appears that Ti does stabilise SSFs to some degree. The higher the Ti content the greater the fault stabilisation and conse-

quently the lower the SSF energy. When the curves of energy versus Ti content shown in figures 6.5 and 6.10 are superimposed (fig. 7.5), it is seen that the APB energy and SESF energy are of the same order in alloys D and G. (The SISF energy was considerably higher than both the SESF and APB energies, therefore deformation by SISFs alone was thought to be unlikely.) Assuming that the dislocation configuration with the lowest total energy will provide the most prolific deformation mode, both super-dislocation and partial dislocation shear would be occurring at 1173K in these two alloys. Although SESFs will form and will be stabilised by Ti, they will only slightly reduce the creep rate because γ' shearing by superdislocations would still occur because an insufficient number of $a/_2$<110> dislocations will be combining to produce the dislocations required for shear by partial dislocations. In support of this only a small increase in stress-rupture life is observed between alloys G and D because the strengthening effect of SSF pinning was annulled by the continuation of superdislocation shear.

Figure 7.5 shows that at 1170K in alloy A the SESF energy is lower than the APB energy, therefore it is easier to form SESFs than APBs and the partial dislocation configuration will have the lowest energy. Consequently deformation by superdislocations is much less likely. As a result of this nearly all deformation will be by partial dislocation shear. The glide of partial dislocations bounding SESFs and SESF/SISF pairs will be retarded by fault stabilisation due to Ti. This will increase the shear resistance of the γ' and as observed for alloy A the stress-rupture life should be increased.

These observations support the hypothesis (Roome, 1982 and fig. 1.14b) that for a given test condition - Roome used 760MPa at 1033K and this investigation used 410MPa at 1123K - partial dislocation shear occurs at lower temperatures with increasing Ti content and that the early onset of partial dislocation shear increases stress-rupture life. Using the

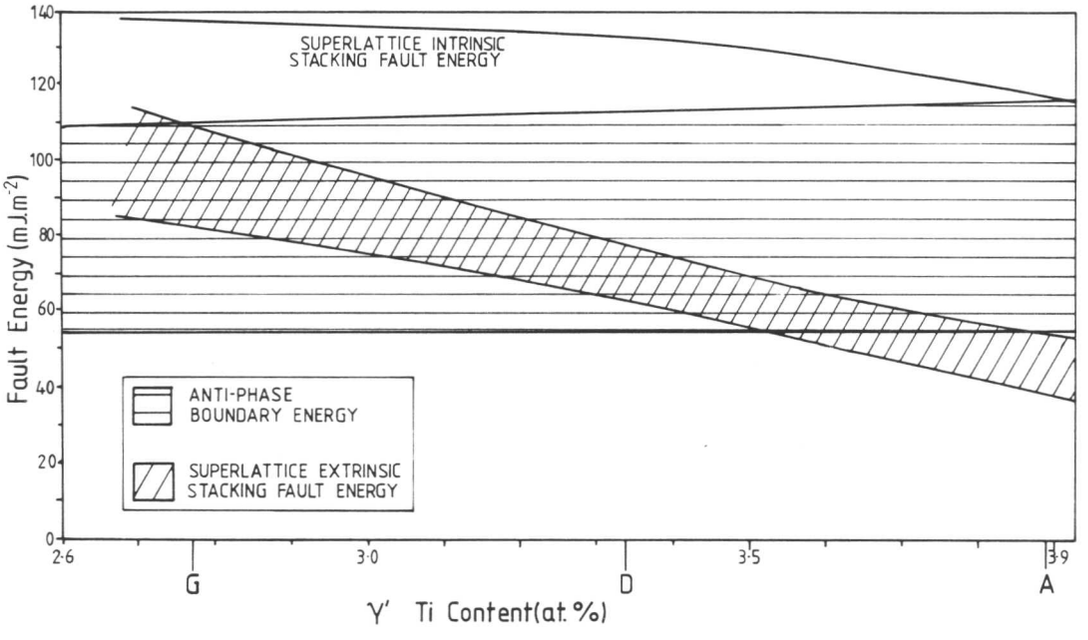

Fig. 7.5. The variation of the APB energy and the SSF energies versus γ' titanium content for alloys A, D and G.

results of this investigation this effect has now been explained by the observed drop in SESF energy lowering the partial dislocation configuration energy to a value below the superdislocation configuration energy with increasing Ti. This is brought about by the segregation of Ti stabilising faults; perhaps by forming thin planar regions on the SSFs which have the Ni_3Ti structure. A schematic representation of the relationship between deformation mechanism, temperature and titanium content proposed as a result of this investigation is shown in figure 7.6. For alloys based on A, D and G the change from mixed shear to partial dislocation shear occurred when the γ' Ti content was approximately 3.7at.% (which is equivalent to an overall Ti content of about 2.6at.%). The best intermediate temperature stress-rupture resistance in this series of alloys will be obtained with alloys which contain greater than 2.6at.% Ti.

The properties are unlikely to continue to improve if considerably larger amounts of Ti are added as these may have a deleterious effect on other properties such as alloy phase stability.

7.6 The Effect of Changes in Strain Rate and Creep Activation Energy Predicted from the Modified Deformation Model

(i) Strain rate

At a given test temperature the fault pinning mechanism may be related to the strain rate. At low strain rates (i.e. in creep), dislocations will be moving fairly slowly through the γ' so sufficient time will be available for Ti to diffuse to and stabilise the moving dislocations. At high strain rates (i.e. in tensile tests) Ti diffusion cannot keep up with the dislocations (assuming the dislocation velocity is increasing with strain rate), and effective pinning will not occur.

At high temperatures Ti diffusion will be more rapid and fault stabilisation can occur more easily. Hence fault stabilisation will be effective to high strain rates. At very high temperatures, however, fault

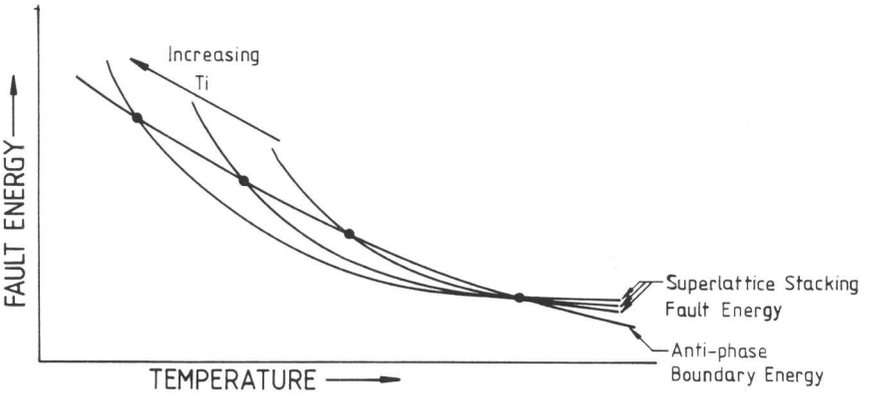

Fig. 7.6. A schematic illustration of the predicted variation in fault energy with titanium content proposed as a result of this investigation.

stabilisation will be ineffective at all strain rates because it will not be thermodynamically favourable for segregation to faults to occur. At low temperatures fault stabilisation will be inoperative because there will not be enough Ti diffusion to form atmospheres on the faults.

(ii) Activation energy

Tien, Kear and Leverant (1972) report that the activation energy for primary creep in single crystal superalloys at 1033K is about 220kJmol^{-1}. They also report that this value increases to about 650kJmol^{-1} when the specimen enters secondary creep, with no obvious change in deformation mechanism. They explain the low value in primary creep by suggesting that it is controlled by vacancy diffusion. They then suggest that the onset of secondary creep coincides with the exhaustion of vacancy diffusion leading to a rise in the activation energy to that characteristic of interstitial diffusion. It is suggested that this mechanism is highly unlikely; interstitial diffusion is only significant for large atoms very close to the melting point.

It may be possible to explain the large increase in activation energy using the model proposed here. It is suggested that at intermediate temperatures in primary creep glide deformation of the γ' is occurring by partial dislocation shear of dislocation combinations present in the structure. The activation energy for this process will be approximately equivalent to the diffusion of Ti in the γ' because the rate controlling step will be Ti diffusion which is required to allow the stabilised stacking faults to move. Secondary creep may begin when the initial dislocation configurations are exhausted. The activation energy will increase to that for dislocation climb in the γ because the rate controlling step will now be dislocation climb to form new dislocation combinations which can glide into the γ'. The application of this mechanism may explain the large increase in activation energy observed by Tien et al. (1973) while maintaining the same deformation mechanism.

Much further work is necessary in order to show that the strain rate sensitivity and activation energies follow the patterns proposed here.

7.7 Summary

Previously it has been shown that Ti stabilises the SSFs by stabilising the region of Ni_3Ti stacking on the fault plane. In this chapter a modification to the established deformation mechanism is suggested where the SSFs formed during partial dislocation shear are stabilised by the diffusion of Ti to the faults. It is also shown that this mechanism may be related to strain rate and creep activation energies, and suggested that experiments should be performed to confirm this.

Chapter 6 shows that the SSF energy decreases with increasing titanium content and this observation has been related to the stress-rupture properties of alloys A, D and G. It is shown here that the modified mechanism can be used to explain the increase in stress-rupture life between alloys D and A when stressed at 430MPa and 1123K. In the cases of alloys D and G the SESF and APB energies are similar and shear of the γ' will occur by a mixture of superdislocation and partial dislocation shear; locking of the SSFs is ineffective because superdislocations are still readily formed. In alloy A the SESF energy is lower than the APB energy and it is predicted that γ' shear occurs by SESF ribbons and SESF/SISF pairs, where the SSFs are strongly pinned. This produces a considerable increase in stress-rupture life because superdislocations cannot form and γ' shear is considerably decreased.

A similar but less pronounced trend is observed at 710MPa and 1023K but it is impossible to draw any conclusion about the effect of the fault energies on this curve as no values have been measured near this temperature. It is suggested that the increase in properties is also due to some change in the proportions of superdislocation shear and partial dislocation shear with increasing temperature.

The tests at 225MPa and 1223K show a gradual increase in life with increasing titanium content. Again, it is impossible to draw any conclusions about the deformation mechanism but it is thought that the APB energy is lower than that at 1123K and the fault pinning mechanism is less effective than at 1123K because the temperature may be high enough for the formation of Ni_3Ti to be energetically unfavourable.

It was not possible to verify the predictions made in this chapter because no TEM was performed on interrupted stress-rupture test specimens and energy results were only measured at one temperature. It would be interesting to examine crept microstructures, measure the activation energies and study the diffusion rates of alloying elements in superalloys as this would add to the knowledge of alloy deformation behaviour. It would also be interesting to measure the energies of APBs and SSFs at a range of temperatures and compare these values with observations of crept microstructures. In this way it would be possible to build up a picture of alloy deformation in creep.

It is clear from the work reported in this thesis that titanium has a major strengthening effect in Ni-base single crystal superalloys. Further research ought to be carried out in a similar way to examine the strengthening role played by other alloying elements such as tantalum and niobium.

CHAPTER 8

CONCLUSIONS AND SUGGESTIONS FOR FURTHER WORK

The major conclusions from this work are summarised below with some suggestions for further research.

8.1 Conclusions

8.1.1 Homogenisation

The single crystal alloys studied achieve adequate homogeneity after annealing for 32 hrs at 157OK. This homogeneity is both long range and on the level of individual γ' particles.

After homogenisation the misfit between extracted γ and γ' is found to be negligible. It is concluded that variation of the Ti content between 1.8at.% and 2.7at.% has no effect on the misfit, presumably because the Ti content of both the γ and the γ' increases by a similar amount through the alloy series.

The γ/γ' misfit and the γ' composition are not perceptibly changed when the γ' particles are coarsened to about 0.5μm by treating for 16 hrs at 139OK.

The heat treatment of 36 hrs at 157OK followed by 16 hrs at 139OK produces specimens with the same γ' volume fraction, γ' particle size and γ/γ' misfit. There is presumably also a negligible difference in the solid solution strengthening of the matrix.

8.1.2 Dislocation interactions

An extension of the mechanism proposed to describe the formation of three-fold nodes in FCC metals (Whelan, 1959) has been used to describe the formation of three-fold supernodes and hexagonal dislocation networks in Ll_2 ordered structures. Weak beam dark field TEM shows that the proposed

mechanism adequately explains the experimental observations.

It is found that two different a<110> superdislocations gliding on the same or different {111} planes can combine to form a third a<110> dislocation and produce two three-fold supernodes and the dislocation intersections. Many interactions produce arrays of screw superdislocations in hexagonal networks. Two different supernodes are produced, one consisting of $a/_6$<211> partial dislocations and complex faults, and the other consisting of $a/_2$<110> dislocations and APBs. In most cases the nodes extend to form alternate regions of intrinsic and extrinsic superlattice stacking fault at the nodal points. The dislocations between the faulted and unfaulted crystal are shown to be $a/_3$<211> partial dislocations, while the boundaries between APBs and SSFs are shown to be $a/_6$<211> partial dislocations. The extended superlattice extrinsic stacking faults (SESF) have larger areas than the extended superlattice intrinsic stacking faults (SISF).

Superdipoles have also been observed in deformed and annealed specimens and two mechanisms are proposed for their formation. These mechanisms are extensions of those proposed for dipole formation in disordered FCC materials. Superdipoles are shown to consist of a loop of APB bounded by like $a/_2$<110> dislocations.

Square dislocation networks lying either on two intersecting {111} planes or on one {001} plane are reported. These seem to form by the intersection of $a/_2$<110> dislocation pairs with Burgers vectors which intersect at 90° gliding on {111} planes. An area of unfaulted crystal is created at the point of intersection. This region is stable and locks the network. At high temperatures the {111} network may cross-slip onto a {001} plane where the APB energy is lower, thus forming a lower energy network.

Large planar defects are observed. TEM analysis shows these to be equivalent to SESFs bounded by $a/_3$<211> partial dislocations. A

mechanism for their formation is proposed. It is noted that the SESF is equivalent to seven layers of the Ni_3Ti structure. It is proposed that titanium diffuses to the faults and stabilises them by forming planar regions of Ni_3Ti. Alloy A, which has the highest Ti content, contains the largest number of planar faults.

8.1.3 The effect of titanium on fault energy

No significant variation is found in the APB energy of γ' with titanium content in single crystal superalloys containing between 1.8 and 2.7at.% titanium. There is, however, a large range of values for each alloy. The mean APB energy using anisotropic elasticity is $83\pm20 mJm^{-2}$ for screw superdislocations at about 1170K. The large range of values may be due to a small contraction of the APB during cooling from 1170K. If this does occur it will raise the APB energy above the value at 1170K.

A new method has been presented for the determination of SSF energy from the extended three-fold supernodes of the superdislocation networks. The method enables the determination of SSF energies as a function of node shape and size.

It is found that the SSF energies decrease with increasing titanium content. The mean SESF energies at 1170K are 94±15, 74±10 and $46\pm12 mJm^{-2}$ for alloys G, D and A respectively while the equivalent SISF energies are 137, 131±10 and $117\pm5 mJm^{-2}$ respectively. The SESF energy is considerably lower than the SISF energy in all cases.

It is proposed that the differences in SSF energy are due to fault stabilisation by the segregation of Ti to the faults. Calculations indicate that bulk diffusion of Ti to the centre of a particle of $Ni_3(Al_{0.6}Ti_{0.4})$ takes about 16 minutes at 1173K. Owing to the complex composition bulk diffusion is likely to be slower in the γ' of the alloys studied, but it is thought that equilibrium is achieved in less than 16 hrs. The SSFs may be stabilised by the formation of Ni_3Ti on the fault plane although no evidence for this has been obtained. The Ti stabilised SESF energy is lower than

the Ti stabilised SISF energy because the SESF is equivalent to a thicker region of the Ni_3Ti than the SISF.

8.1.4 The effect of titanium on superalloy deformation

It is proposed that the wide SSFs and SSF pairs observed by other workers in the partial dislocation shear régime can be explained in terms of fault stabilisation by Ti. No change to the dislocation configurations is suggested but it is thought that Ti diffuses to the faults and stabilises them. In the appropriate temperature range stabilised faults are effectively pinned by the Ti: the mechanism can be likened to Suzuki locking. Glide of the partial dislocations cannot continue unless the stabilising Ti diffuses with the fault or the fault can break away from the stabilising atmosphere. Using data for $Ni_3(Al_{0.6}Ti_{0.4})$ and a secondary creep rate of alloy A, it is shown that Ti diffusion can keep up with partial dislocation glide at temperatures above 630K. This temperature is expected to be higher for the γ' of alloys A, D and G because they contain elements such as Ta and W which should considerably reduce Ti diffusion.

Tests show that the stress-rupture life improves with increasing Ti in all conditions. This improvement is most obvious at 1123K and 410MPa. The SESF energies in alloys D and G lie within the band of APB energies but that SESF energy is lower than the APB energy in alloy A. The stress-rupture life of alloy A is considerably longer than that of alloy G. It is suggested that alloys D and G deform by a combination of superdislocation shear and partial dislocation shear. SESF stabilisation by Ti will occur but slip can still readily occur by the passage of superdislocations. In alloy A, however, the dislocation interactions necessary to produce SESFs will occur more readily than those to produce APBs. γ' shear will occur mainly by partial dislocation glide but this will be retarded by the stabilisation of SESFs by Ti. This effect may produce the large difference in properties between alloys A and G.

It is predicted that at a given test temperature stress-rupture

life is improved if enough Ti is added to produce stabilised SSF configurations with lower energies than the APB configurations. Adding Ti lowers the temperature of the change from superdislocation shear to partial dislocation shear. When more than 2.6at.% Ti is added the SESF energy is lower than the APB energy and it is thought that deformation by partial dislocation shear predominates at 1170K. This can then lead to an increase in stress-rupture life over a similar alloy with a Ti content less than 2.6at.%.

It has been shown that contrary to the predictions of other workers Ti lowers the SSF energies relative to the APB energy, the latter being unaffected by Ti content within the limits of experimental error.

8.2 Suggestions for Further Work

8.2.1 Homogenisation

Detailed theoretical modelling of the homogenisation process is desirable since the heat treatment window and defect energies depend critically on compositional variations. It is anticipated that the problem may be very difficult since the model must treat complex multi-component diffusion and very few superalloy diffusion data are available. However, it may be possible to simplify the system by approximating it to a binary or a ternary system.

The misfit between extracted γ and γ' at room temperature was found to be negligible but it may depend on temperature. It would be interesting to measure the thermal expansivity of the two phases, using a dilatometer, either as extracts or by manufacturing alloys with γ and γ' compositions. In this way it may be possible to determine if misfit strengthening is related to temperature.

8.2.2 Deformation mechanisms

It has been observed that the SSF energies decrease with increasing Ti content. It is proposed that this is due to Ti migrating to, and

stabilising, the SSFs. However, the operation of this process could not be properly confirmed because very few data are available for the diffusion coefficients and activation energies for elemental self-diffusion in the γ' of complex alloys. It is vital to the development of the ideas proposed in this thesis that this lack of data is rectified. The most useful values would be those for Ti diffusion; these could perhaps be found by the use of radioactive tracer techniques to follow Ti diffusion at various temperatures in an alloy with the γ' composition.

The creation and analysis of superdislocation networks and the formulation of a method to evaluate the SSF energies from extended supernodes has established a technique for the evaluation of APB and SSF energies in ordered materials. This investigation has been limited to small variations in one alloy component at one temperature. It is now up to other workers to study the effect of temperature on fault energies either by heat treating networks for long periods at different temperatures and then examining them at room temperature in the TEM, or by studying the behaviour of the networks using a heating stage in the TEM to watch changes in the supernodes in situ.

Further work should also be considered to study the effect of other alloying elements (for example, Nb and Ta) which are thought to affect superalloy strength by changing the fundamental defect energies.

Many interesting and unusual dislocation configurations have been observed in deformed and annealed superalloy microstructures but many have not been analysed. A considerable amount of work could be undertaken to study these other interactions. It would also be interesting to carefully control the deformation of samples to find how stress and strain rate affect the dislocation interactions produced, particularly the hexagonal networks.

Contributions to alloy strengthening by dislocations by-passing the γ' particles have been largely ignored by workers studying superalloy

deformation. Most recent improvements in superalloy strengthening mechanisms act to reduce dislocation glide through the γ' by lowering the SSF energy and cause partial dislocation glide. This process increases the dislocation density in the γ matrix. At intermediate and high temperatures it is likely that many un-paired dislocations climb around the γ' particles because the γ cannot glide through. It is suggested that it would be useful to study dislocation behaviour in the γ region of high γ' volume fraction superalloys and relate this behaviour to alloy strengthening, particularly at high temperatures.

The literature contains a considerable amount of data for flow stresses measured from high strain rate tensile tests but very little data for low strain rate creep and stress-rupture tests. This seems strange as most service failures of turbine blades occur in creep. It is suggested that more investigations of the type undertaken here should be performed to study the effect of alloy composition on deformation mechanisms and defect energies. Studies should also be undertaken to study deformation mechanisms during creep by the TEM examination of foils manufactured from interrupted test specimens. Experiments of this type could be used to build up an overall picture of creep properties which relates alloy composition, strain rate, temperature and deformation mechanism.

Up to the present time superalloy design has been largely empirical but to gain further improvements in superalloy properties the effects of specific elements on alloy behaviour need to be studied closely if alloys with the optimum properties for their applications are to be produced. Single crystal superalloys will be useful tools in the search for improved superalloys because they can be fully homogenised, they contain very little carbon and no grain boundaries. This means that it is possible to study the effect of small changes in alloy composition on behaviour without the effects of inhomogeneities introduced by factors such as grain boundary segregation and carbide precipitation.

Appendix A. Stress-rupture Test Results

Test conditions		Alloy	Life to failure (hrs)
Stress (MPa)	Temperature (K)		
710	1023	A 1	337.2
		2	336.2
		D 1	217.1
		2	216.4
		3	194.3
		G 1	176.2
		2	136.3
430	1123	A 3	197.8
		4	217.0
		5	235.8
		D 4	118.0
		5	113.9
		6	107.8
		G 3	117.8
		4	98.5
		5	113.4
225	1223	A 6	181.0
		7	190.2
		D 7	164.9
		8	138.1
		9	130.9
		G 6	115.2
		7	100.4

Appendix B. Calculation of the Homogenisation Time Using $X=\sqrt{Dt}$

This simple calculation has been performed by approximating inhomogeneous as-cast material to a binary FCC solid solution of nickel with the most severely segregated element, in this case tungsten.

Figure B.1 shows an SEM/EDS trace of the distribution of tungsten across three dendrite arms.

According to Walsh and Donachie (1969) between 1273 and 1589K the diffusion coefficient for tungsten in nickel is:

$$D_W = 1.19\times10^{-4}\exp(-0.0469c_W)\exp(\frac{-3.69\times10^4}{T})m^2s^{-1} \qquad \text{eqn. B.1}$$

where T is the homogenisation temperature and c_W is the tungsten concentration.

The homogenisation temperature used is 1573K and the overall alloy tungsten content is 2·8 at.%. This gives a value of $6{\cdot}77\times10^{-15}$ m^2s^{-1} for the diffusion coefficient.

Substituting this value in $X=\sqrt{Dt}$ where X is the maximum distance a tungsten atom is required to diffuse and t is the time taken for complete homogenisation.

From figure B.1 X=32μm

$$t = \frac{X^2}{D} = 42{\cdot}02\,\text{hrs} \qquad \text{eqn. B.2}$$

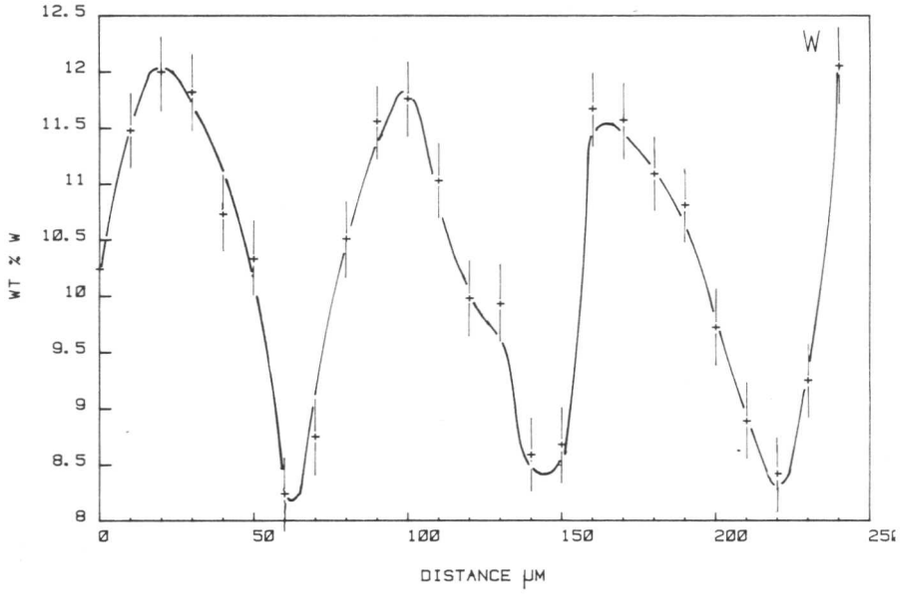

Fig. B.1. SEM/EDS analysis trace for tungsten taken across three dendrite arms of as-cast alloy A.

Appendix C. Comments on the Analysis Data Produced by the Link 860

Tables 2.1 and 2.2 show that there are considerable variations in the analysed Al contents of the γ and γ' obtained from the homogenised alloys by the Philips 400T and Link 860 analysis system. It is thought that this variation may be caused by the background subtraction performed by the Link 860. To find the background count level the system assesses the counts at either end of an analysis window which includes the peak it is analysing. It then uses these end points to calculate the background level under the peak and subtracts this from the gathered symbol to leave the counts collected from the element it is analysing.

It can be seen from figure C1 that for the alloys studied the Ta and W M_α peaks are close to the Al K_α peak and that they are situated at one end of the sampling window. The presence of the Ta and W peaks may cause the Link software to assess an incorrect Al background. Compared to Ta and W, Al is a light element and small changes in the background caused by small changes in the Ta and W may produce considerable errors in the Al content calculated by the Link.

More accurate Al data will be gained if the background assessment window is narrowed to avoid the Ta and W peaks or if the Ta and W M_α peaks are subtracted before the Al background is assessed.

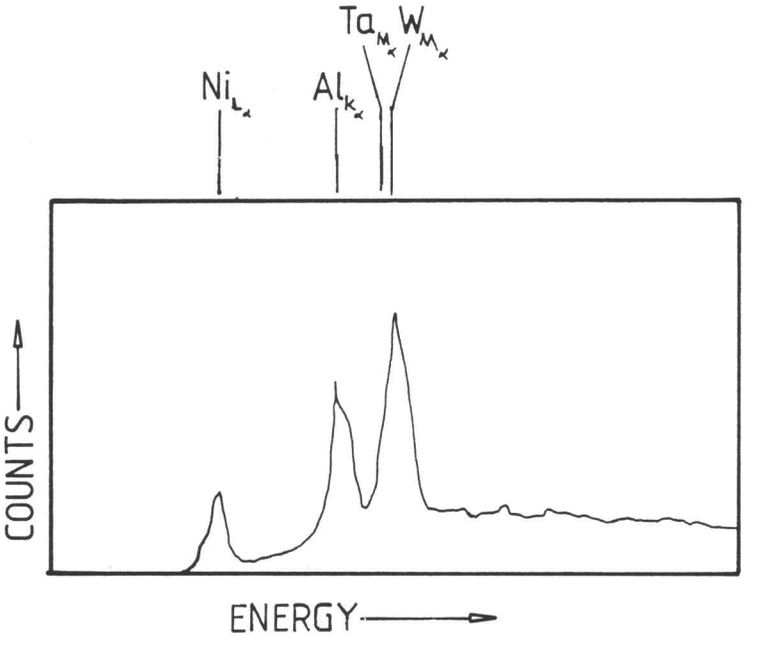

Fig. C.1. Section from an EDS spectrum gathered from the γ' of a fully homogenised thin foil of alloy A. Note the close proximity of the W and Ta M_α peaks to the Al K_α peak.

Appendix D. Calculation of the Superlattice Stacking Fault Energy from Extended Supernodes (After Rae, 1984)

Equations representing the stress field of each of the screw dislocation segments shown in figure D.1 are used to calculate the total stress field on a point O on dislocation 6. The stress field for each dislocation is calculated using a separate co-ordinate system (x_j, y_j, z_j) for each dislocation where the z_j axis lies along the dislocation line and the x_j axis is normal to the plane of the node. The stress fields due to each dislocation are then resolved on the co-ordinate system (X, Y, Z) of dislocation 6 to calculate the force on that dislocation.

The only non-zero component for the Burgers vector of a screw dislocation is b_z. Thus the only non-zero stress component is σ_{xz} (Hirth and Lothe, 1982) which will subsequently be referred to as σ_j, the stress on dislocation j:

$$\sigma_j = \frac{\mu\, b_j}{4\pi} \frac{y}{M(M+L)} \qquad \text{Eqn. D.1(a)}$$

where μ is the isotropic shear modulus taken to equal $[C_{44}(C_{11}-C_{12})/2]^{\frac{1}{2}}$, $M^2=x^2+y^2+(z-z_j)^2$, $L=z_j-z$, y and z are the co-ordinates of O relative to the axes based on the segment under consideration and z_j and z_j' are the end points of the dislocation under consideration.

It follows that:

$$\sigma_j(z_j) = \frac{\mu b_j}{4\pi}\left[\frac{y}{(y^2+(z-z_j)^2)^{\frac{1}{2}}((y^2+(z-z_j)^2)^{\frac{1}{2}}+(z_j-z))}\right] \qquad \text{Eqn. D.1(b)}$$

Consequently the stress on dislocation i from z_j to z_j' is

$$\sigma_j = \sigma_j(z_j)-\sigma_j(z_j').$$

It is assumed that dislocations 4 and 5 have infinite length. The stress fields of dislocations 7 and 8 have no component in

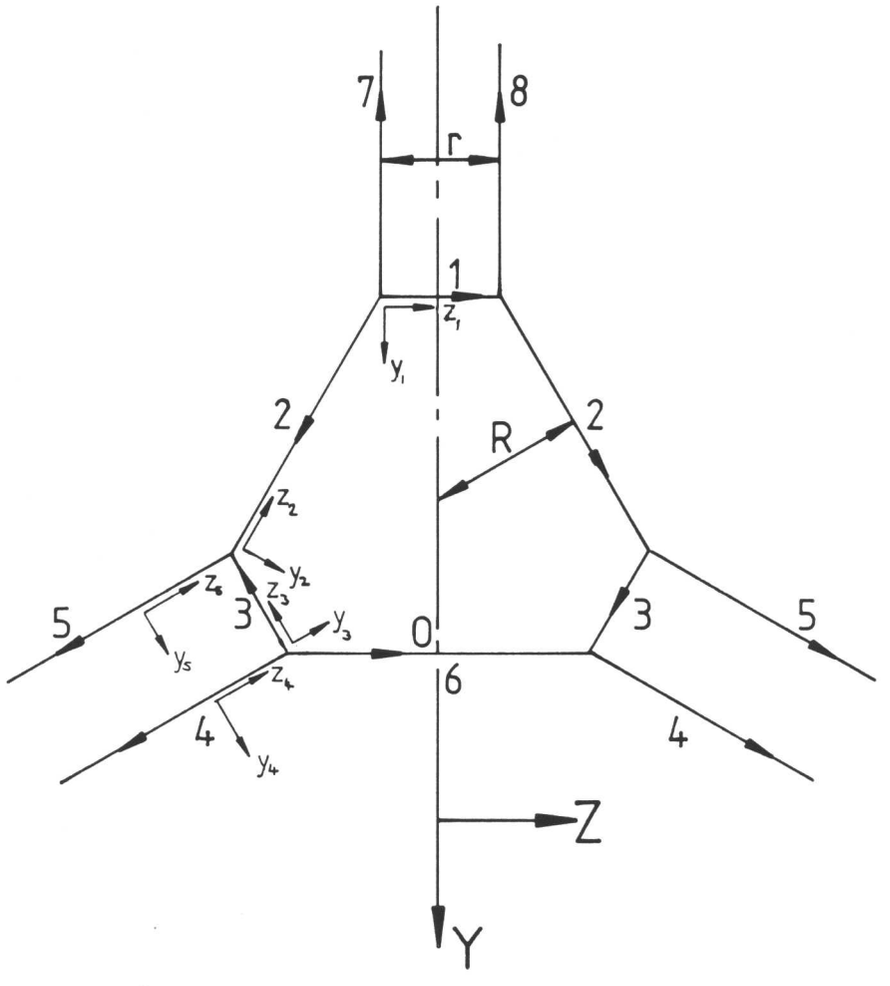

Fig. D.1. Dislocation configuration at a supernode showing the co-ordinate axes used to evaluate the stress field of each dislocation.

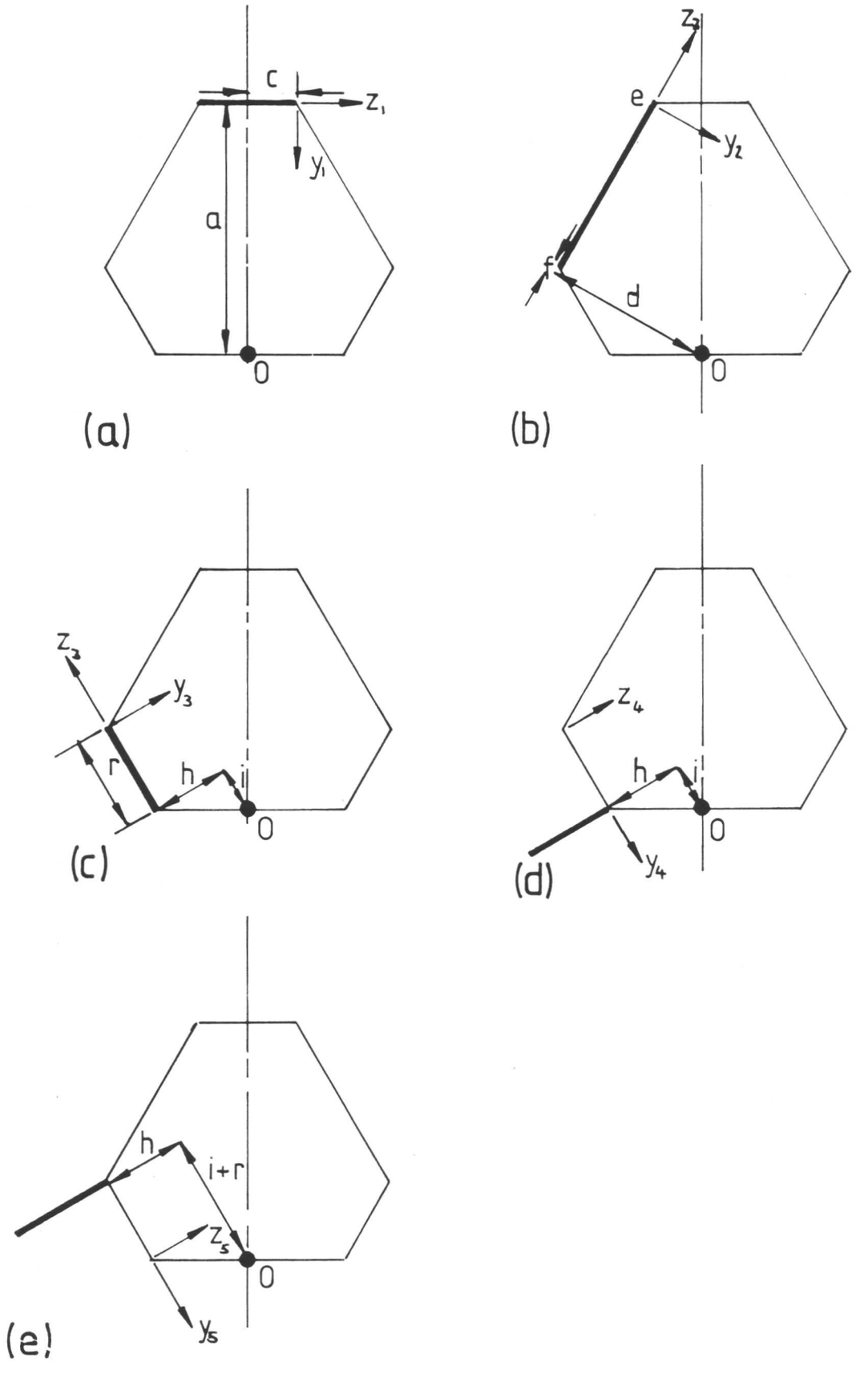

Fig. D.2. Illustration showing the co-ordinate systems and parameters used to evaluate the stress field of dislocation 1, (a); dislocation 2, (b); dislocation 3, (c); dislocation 4, (d); and dislocation 5, (e).

the Z reference direction so they have no effect on the calculation and can be ignored.

Stress on dislocation 1 (fig. D.2a)

Co-ordinates of dislocation origin:

$$x=0,\ y=a,\ z=0$$

limits:

$$z_1=-c,\ z_1'=+c$$

$$\sigma_1 = \frac{\mu b}{4\pi}\left[\frac{2c}{a(a^2+c^2)^{\frac{1}{2}}}\right] \qquad \text{eqn. D.3(a)}$$

In terms of the node dimensions R and r:

$$a = 3R-\frac{\sqrt{3}r}{2} \text{ and } c = \frac{r}{2}$$

Substituting these in eqn. D.3(a) gives:

$$\sigma_1 = \frac{\mu b_1}{4\pi}\left[\frac{r}{(3R-\frac{\sqrt{3}r}{2})(9R^2-3\sqrt{3}Rr+r^2)^{\frac{1}{2}}}\right] \qquad \text{eqn. D.3(b)}$$

Stress on dislocation 2 (fig. D.2b)

Co-ordinates of dislocation origin:

$$x=0,\ y=d,\ z=\pm f$$

limits:

$$z_2=0,\ z_2'=e$$

$$\sigma_2 = \frac{\mu b_2 d}{4\pi}\left[\frac{1}{(d^2+(e-f)^2)^{\frac{1}{2}}[(d^2+(e-f)^2)^{\frac{1}{2}}+(e-f)]} - \frac{1}{(d^2+f^2)^{\frac{1}{2}}[(d^2+f^2)^{\frac{1}{2}}-f]}\right] \qquad \text{eqn. D.4(a)}$$

In terms of the node dimensions:

$$d=\frac{3R}{2},\ e=2(\sqrt{3}R-r),\ f=(\frac{\sqrt{3}R}{2}-r)$$

Substituting these in eqn. D.4(a) gives:

$$\sigma_2 = \frac{3\mu b_2 R}{8\pi}\left[\frac{1}{(9R^2-3\sqrt{3}Rr+r^2)^{\frac{1}{2}}[(9R^2-3\sqrt{3}Rr+r^2)^{\frac{1}{2}}+\frac{3}{2}\sqrt{3}R-r]}\right.$$

$$\left. - \frac{1}{(3R^2-\sqrt{3}Rr+r^2)^{\frac{1}{2}}[(3R^2-\sqrt{3}Rr+r^2)^{\frac{1}{2}}-(\frac{\sqrt{3}}{2}R-r)]}\right] \qquad \text{eqn. D.4(b)}$$

Stress on dislocation 3 (fig. D.2c)

Co-ordinates of dislocation origin:

$$x=0,\ y=h,\ z=-i$$

limits:

$$z_3=0,\ z_3'=r$$

$$\sigma_3 = \frac{\mu b_3 h}{4\pi}\left[\frac{1}{(h^2+(r-i)^2)^{\frac{1}{2}}[(h^2+(r+i)^2)^{\frac{1}{2}}+r+i]} - \frac{1}{(h^2+i^2)^{\frac{1}{2}}[(h^2+i^2)^{\frac{1}{2}}+i]}\right] \qquad \text{eqn. D.5(a)}$$

In terms of the node dimensions:

$$h^2+(r+i)^2 = [3R^2-\sqrt{3}Rr-4r^2]\ ;$$

$$h^2+i^2 = (\sqrt{3}R-r)^2 \quad ; \quad h = \frac{3R-\sqrt{3}r}{2}$$

Substituting these in eqn. D.5(a) gives:

$$\sigma_3 = \frac{\mu b_3(3R-\sqrt{3}r)}{8\pi}\left[\frac{1}{(3R^2-\sqrt{3}Rr+r^2)^{\frac{1}{2}}\left[(3R^2-\sqrt{3}Rr+r^2)^{\frac{1}{2}}+\frac{\sqrt{3}R+r}{2}\right]} - \frac{1}{\frac{3}{2}(\sqrt{3}R-r)^2}\right] \qquad \text{eqn. D.5(b)}$$

Stress on dislocation 4 (fig. D.2d)

Co-ordinates of dislocation origin:

$$x=0,\ y=i,\ z=h$$

limits:

$$z_4=0,\ z_4'=\infty$$

$$\sigma_4 = \frac{\mu b_4 i}{4\pi} \frac{1}{(i^2-h^2)^{\frac{1}{2}}[(i^2+h^2)^{\frac{1}{2}}+h]} \qquad \text{eqn. D.6(a)}$$

but:

$$(i^2+h^2)^{\frac{1}{2}} = 2i \quad ; \quad h = \sqrt{3}i$$

In terms of the node dimensions:

$$i = \frac{(\sqrt{3}R-r}{2}$$

Substituting eqn. D.6(a) gives:

$$\sigma_4 = \frac{\mu b_4}{4\pi} \frac{1}{(\sqrt{3}R-r)(2+\sqrt{3})} \qquad \text{eqn. D.6(b)}$$

Stress on dislocation 5 (fig. D.2e)

Co-ordinates of dislocation origin:

$$x=0, \; y=(i+r), \; z=h$$

limits:

$$z_5=0, \; z_5'=\infty$$

$$\sigma_5 = \frac{+\mu b_5 (i+r)}{4\pi} \left[\frac{1}{((i+r)^2+h^2)^{\frac{1}{2}}[((i+r^2)+h^2)^{\frac{1}{2}}+h]} \right] \qquad \text{eqn. D.7(a)}$$

In terms of the node dimensions:

$$i+x = \frac{\sqrt{3}R+r}{2} \quad ; \quad h = \frac{3R-\sqrt{3}r}{2}$$

Substituting in D.7(a) gives:

$$\sigma_5 = \frac{\mu b_5}{8\pi} \left[\frac{(\sqrt{3}R+r)}{(3R^2-\sqrt{3}Rr+r^2)^{\frac{1}{2}} \left[(3R^2-\sqrt{3}Rr+r^2)^{\frac{1}{2}} + \frac{3R-\sqrt{3}R}{2} \right]} \right] \qquad \text{eqn. D.7(b)}$$

Resultant resolved stress on dislocation 6

The resultant resolved force, F, on dislocation 6 is the sum of the stresses on all the component dislocation segments resolved along Z_6:

$$F = [\sigma_1+2\sigma_2\cos60-2\sigma_3\cos60+2\sigma_4\cos30+2\sigma_5\cos30].b_6$$

$$F = [\sigma_1+\sigma_2-\sigma_3+\sqrt{3}\sigma_4+\sqrt{3}\sigma_5]\cdot b_6 \qquad \text{eqn. D.8}$$

So, equating this with the SSF energy of the supernode gives:

$$\gamma_{SSF} = [\sigma_1+\sigma_2-\sigma_3+\sqrt{3}\sigma_4+\sqrt{3}\sigma_5]\cdot b_6 \qquad \text{eqn. D.9}$$

Appendix E. Anti-phase Boundary Energy Results

Alloy A (γ' Ti content = 3.9 at.%)

Dislocation Spacing (nm)	Energy (mJm^{-2})
8.4	86
6.75	107
6.56	110
10.5	69
8.36	86
8.55	85
6.35	114
9.32	78
9.42	77
9.17	78
10.39	70
9.30	78
8.78	83
9.12	80
10.61	68
7.95	91
10.11	71
12.12	60
7.21	100
9.74	74

Alloy D (γ' Ti content = 3.3 at.%)

Dislocation Spacing (nm)	Energy (mJm^{-2})
6.36	114
11.27	64
13.13	55
8.02	90
8.02	90
10.26	70
10.31	70
8.75	83
10.00	72
10.47	69

Alloy G (γ' Ti content = 2.8 at.%)

Dislocation Spacing (nm)	Energy (mJm^{-2})
7.54	96
6.70	108
6.29	115
6.29	115
12.66	57
12.66	57
8.89	81
8.51	85
9.14	79
9.14	79
9.89	73
7.44	97

Appendix F. Superlattice Stacking Fault Energy Results

Intrinsic supernodes

Alloy	Dislocation Spacing r (nm)	Internal Radius R (nm)	ρ (r/R)	Energy γ_{SISF} (mJm^{-2})
A	9	6.5	1.38	117
(γ'Ti=3.9 at.%)	9	6.5	1.38	117
	9	6.5	1.38	117
	9	6.5	1.38	117
	9	6.5	1.38	117
	9	6.5	1.38	117
	8	6.0	1.33	119
D	9	6	1.5	134
(γ'Ti=3.3 at.%)	9	6	1.5	134
	9	6.5	1.38	117
	9	6	1.5	134
	9	6	1.5	134
	9	6	1.5	134
G				
(γ'Ti=2.8 at.%)	6	5	1.2	137

Extrinsic supernodes

Alloy	Dislocation Spacing r (nm)	Internal Radius R (nm)	ρ (r/R)	Energy γ_{SESF} (mJm^{-2})
A	9	12	0.75	55
(γ'Ti=3.9 at.%)	9	14	0.64	47
	9	16.5	0.55	40
	9	14	0.64	47
	9	13.5	0.66	49
	9	14.4	0.62	45
	8	13.5	0.59	49
	8	17	0.47	39
D	9	9.5	0.95	70
(γ'Ti=3.3 at.%)	9	8.5	1.06	79
	9	9	1	74
	9	9	1	74
	9	8.5	1.06	79
	9	9	1	74
	6.5	10.5	0.62	63
	9	9	1	74
	9	8.5	1	79
G	5	7.5	0.67	88
(γ'Ti=2.8 at.%)	5	7	0.71	94
	6.5	6.5	1	100
	7	8	0.88	82
	10	7	1.43	108

Appendix G. Calculation of the Minimum Temperature at which Titanium Diffusion is Rapid Enough to Move with a Pair of $a/_3$<211> Dislocations

Consider the dislocation density, ρ, to be about $10^{13}m^{-2}$, the total Burgers vector of the dislocation bounding the fault to be $\underline{b}$=a<110> and the secondary creep rate, $\dot{\varepsilon}$, (measured from alloy A) to be $6x10^{-8}s^{-1}$. When the gamma prime lattice parameter is 0.358nm the magnitude of b is about $5x10^{-10}m$.

The velocity of the gliding dislocation, v, is:

$$v = \frac{\dot{\varepsilon}}{\rho b} = 1.2x10^{-11}ms^{-1}. \qquad \text{eqn. G.1}$$

So in one second the dislocations will move $1.2x10^{-11}m$.

If titanium is to pin the dislocation it must also travel $1.2x10^{-11}m$ in one second.

Now, according to Larikov et al. (1982), the diffusion coefficient for titanium diffusion in $Ni_3(Al_{0.6}Ti_{0.4})$ is:

$$D = 1.9x10^{-10}\exp\left(\frac{-17462}{T}\right)m^2s^{-1} \qquad \text{eqn. G.2}$$

By substituting this into $\sqrt{Dt}=v$ the minimum temperature at which titanium diffusion is rapid enough to move with the dislocation is found to be 630K.

REFERENCES

E. Aerts, P. Delavignette, R. Siems and S. Amelinckx, 1962, J. Appl. Phys., 33, p3078

S. Amelinckx, 1956, Phil. Mag., 1, p269

S. Amelinckx, 1979, Dislocations in Solids: Volume 2, ed. F.R.N. Nabarro, North-Holland Publ. Co., Amsterdam, p67

I. Baker, D.V. Veins and E.M. Schulson, 1984, J. Mat. Sci., 19, p1799

R. Bakish and W.D. Robertson, 1956, Acta Met., 4, p342

A. Baldan, 1983, Phys. Stat. Sol. (a), 75, p441

C.C. Bampton, I.P. Jones and M.H. Loretto, 1978, Acta Met., 26, p39

B.E.P. Beeston, I.L. Dillamore and R.E. Smallman, 1968, Met. Sci. J., 2, p12

B.E.P. Beeston and L.K. France, 1968, J. Inst. Metals, 96, p105

W. Bell, W.R. Roser and G. Thomas, 1964, Acta Met., 12, p1247

J.D. Bernal, 1969, Science in History: Volume 1, C.A. Watts and Co. Ltd., London, p220

B.A. Bilby, R. Bullough and E. Smith, 1955, Proc. Roy. Soc., A231, p263

D. Blavette and A. Bostel, 1984, Acta Met., 32, p811

L.M. Brown and R.K. Ham, 1971, Strengthening Mechanisms in Crystals, eds. A. Kelly and R.B. Nicholson, App. Sci. Publ. Ltd., London, p9

L.M. Brown and A.R. Thölen, 1964, Disc. Faraday Soc., 38, p35

T. Carnahan, B. Cullen, J. Demel, J. McIlwain, M.J. Marcinkowski, J. Munford, J. Pahlman, T. Prevender and J. Warner, 1967, Trans. Met. Soc. AIME., 239, p2014

C. Carry, C. Houis and J.L. Strudel, 1981, Mem. et Etudes Sci. Rev. de Met., 78, p139

C. Carry and J.L. Strudel, 1975, Scripta Met., 9, p731

C. Carry and J.L. Strudel, 1979, Acta Met., 25, p767

C. Carry and J.L. Strudel, 1978, ibid., 26, p859

B. Chalmers, 1954, Trans. AIMME., 200, p519

J.W. Christian and P.R. Swann, 1967, Alloying Behaviour and Effects in Concentrated Solid Solutions, ed. T.B. Masalski, Gordon and Breach, New York, p105

C.T. Chou, P.B. Hirsch, M. McLean and E. Hondros, 1982, Nature, 300, p621

L.M. Clareborough, 1971, Aust. J. Phys., 24, p79

L.M. Clareborough and A.J. Morton, 1969a, Aust. J. Phys., 22, p351

L.M. Clareborough and A.J. Morton, 1969b, ibid., 22, p371

D.J.H. Cockayne, 1973, J. Microc., 98, p116

D.J.H. Cockayne, M.L. Jenkins and I.L.F. Ray, 1971, Phil. Mag., 24, p1383

D.J.H. Cockayne, P. Pirouz, Z. Liu, G.R. Anstis and P. Karnthaler, 1984, Phys. Stat. Sol. (a), 82, p425

D.J.H. Cockayne, I.L.F. Ray and M.J. Whelan, 1969, Phil. Mag., 20, p1265

S.M. Copley and B.H. Kear, 1967, Trans. Met. Soc. AIME., 239, p984

A.H. Cottrell, 1953, Dislocations and Plastic Flow in Crystals, Oxford University Press, p172

A.G. Cullis and G.R. Booker, 1972, Proc. 5th European Congress on Electron Microscopy, Manchester, Inst. of Phys., London, p532

B.D. Cullity, 1978, Elements of X-Ray Diffraction: 2nd Edition, Addison-Wesley Publ. Co. Inc., London.

J. Czernichow, J.P. Gudas, M.J. Marcinkowski and Wen Feng Tseng, 1971, Met. Trans., 2, p2185

R.G. Davies and N.S. Stoloff, 1965, Trans. AIME., 233, p714

R.F. Decker, 1969, Steel Strengthening Mechanisms, Climax Moly. Co., Zurich, p147

R.F. Decker and J.R. Mihalisin, 1969, Trans. ASM., 62, p481

D. Driver, D.W. Hall and G.W. Meetham, 1981, The Development of Gas Turbine Materials, Applied Science Publishers, London

R.C. Ecob, R.A. Ricks and A.J. Porter, 1982, Scripta Met., 16, p1085

K. Enami and S. Nenno, 1968, J. Phys. Soc. Japan, 25, p1517

J.D. Eshelby, W.T. Read and W. Shockley, 1953, Acta Met., 1, p251

E.A. Fell, 1961, Metallurgia, 63, p157

H. Fisher and M.J. Marcinkowski, 1961, Phil. Mag., 6, p1385

P.A. Flinn, 1960, Trans. Met. Soc. AIME., 218, p145

H. Föll, C.B. Carter and M. Wilkens, 1980, Phys. Stat. Sol. (a), 58, p393

L.K. France and M.H. Loretto, 1968, Proc. Roy. Soc., A307, p83

H.J. Frost and M.F. Ashby, 1982, Deformation-Mechanism Maps, Pergammon Press, Oxford, p57

P.C.J. Gallagher, 1966, Phys. Stat. Sol., 16, p95

R. Gevers, A. Art and S. Amelinckx, 1963, Phys. Stat. Sol., 3, p1563

H. Gleiter and E. Hornbogen, 1965, Phys. Stat. Sol., 12, p251

A.F. Giamei, J.M. Oblak, B.H. Kear and W.H. Rand, 1971, Proc. 29th An. Meeting EMSA, p112

D.A. Grose and G.S. Ansell, 1981, Metall. Trans., 12A, p1631

A. Havalada, 1969a, Trans. ASM, 62, p477

A. Havalada, 1969b, ibid., 62, p581

A.K. Head, P. Humble, L.M. Clareborough, A.J. Morton and C.T. Forwood, 1973, Computed Electron Micrographs and Defect Identification, North-Holland Publ. Co., Amsterdam

P. Hirsch, A. Howie, R.B. Nicholson, D.W. Pashley and M.J. Whelan, 1977, Electron Microscopy of Thin Crystals, 2nd Edition, Butterworths, London

J.P. Hirth and J. Lothe, 1982, Theory of Dislocations, 2nd Edition, J. Wiley and Sons, New York.

E. Hornbogen and M. Mukerjee, 1964, Z. Metallk., 55, p293

L.M. Howe, M. Rainville and E.M. Schulson, 1974, J. Nuc. Mat., 50, p139

A. Howie and C.H. Sworn, 1970, Phil. Mag., 22, p861

A. Howie and M.J. Whelan, 1961, Proc. Roy. Soc., A263, p217

A. Howie and M.J. Whelan, 1962, ibid., A267, p206

W.G. Johnston and J.J. Gilman, 1960, J. Appl. Phys., 31, p632

B.H. Kear, 1966, Acta Met., 14, p659

B.H. Kear, 1974, Proc. Int. Symp. on Order-Disorder Transformations in Alloys, Tubingen, Germany, ed. H. Warlimont, Springer-Verlag, Berlin, p440

B.H. Kear, A.F. Giamei, J.M. Silcock and R.K. Ham, 1968, Scripta Met., 2, p287

B.H. Kear, G.R. Leverant and J.M. Oblak, 1969, Trans. ASM, 62, p639

B.H. Kear and J.M. Oblak, 1974, J. Phys. Coll., 35, pC7-35

B.H. Kear, J.M. Oblak and A.F. Giamei, 1970, Metall. Trans., 1, p2477

B.H. Kear and G.F. Wilsdorf, 1962, Trans. Met. Soc. AIME., 224, p382

P.M. Kelly, A. Jostsons, R.G. Blake and J.G. Napier, 1975, Phys. Stat. Sol. (a), 31, p771

J.M. Kenyon, 1983, Part II project, University of Cambridge

J.S. Koehler and F. Seitz, 1947, J. Appl. Mech., 14, pA-217

L.N. Larikov, V.V. Geichenko and V.M. Fal'chenko, 1981, Diffusion Processes in Ordered Alloys, Amerind Publ. Co. Pvt. Ltd., New Delhi, p117

G.R. Leverant, M. Gell and S.W. Hopkins, 1970, 2nd Int. Conf. on the Strength of Metals and Alloys, ASM, p1141

G.R. Leverant, M. Gell and S.W. Hopkins, 1971, Mat. Sci. Eng., 8, p125

G.R. Leverant and B.H. Kear, 1970, Metall. Trans., 1, p491

G.R. Leverant, B.H. Kear and J.M. Oblak, 1973, Metall. Trans., 4, p355

M.H. Loretto, 1964, Phil. Mag., 10, p467

M.H. Loretto, 1969a, Phil. Mag., 12, p141

M.H. Loretto, 1969b, Phys. Stat. Sol., 35, p167

M.J. Marcinkowski, 1963, Electon Microscopy and Strength of Crystals, eds. G. Thomas and J. Washburn, Interscience, New York, p333

M.J. Marcinkowski, N. Brown and R.M. Fisher, 1961, Acta Met., 9, p129

A.L. Marsh, 1906, U.K. Patent no. 2129

J.R. Mihalisin, 1969, Advances in X-Ray Analysis, 13, p598

R.F. Miller and G.S. Ansell, 1977, Met. Trans., 8A, p1979

W.I. Mitchell, 1966, Z. Metallk., 57, 586

F.R.N. Nabarro, 1967, Theory of Crystal Dislocations, Oxford University Press, p421

P.G. Nash, V. Vejus and W.W. Laing, 1982, Bulletin of Alloy Phase Diags., 3, p367

J.R. Nicholls and R.D. Rawlings, 1977, J. Mat. Sci., 12, p2456

O. Noguchi, Y. Oya and T. Suzuki, 1981, Met. Trans., 12A, p1647

R. Nordheim and N.J. Grant, 1954, Trans. AIMME., 200, p211

J.M. Oblak and B.H. Kear, 1972, Electron Microscopy and the Structure of Materials, Univ. of California Press, London, p566

J.M. Oblak, W.A. Owczarski and B.H. Kear, 1971, Acta Met., 19, p355

J.M. Oblak and W.H. Rand, 1972, Proc. 30th Annual Meeting of EMSA, p648

K. Ono and R. Stern, 1969, Trans. Met. Soc. AIME., 245, p171

E. Orowan, 1948, Symposium on Internal Stress in Metals and Alloys, Inst. of Metals, London, p451

V. Paidar, D.P. Pope and V. Vitek, 1984, Acta Met., 32, p435

H. Pak, T. Saburi and S. Nenno, 1976, Scripta Met., 10, p1081

R.M.N. Pelloux and N.J. Grant, 1960, Trans AIME., 218, p232

B.J. Piearcey, 1970, US Patent no. 3,494,709

B.J. Piearcey, B.H. Kear and R.W. Smashey, 1967, Trans. ASM, 60, p634

B.J. Piearcey and B.E. Terkelson, 1967, Trans. Met. Soc. AIME., 239, p1143

D.P. Pope and S.S. Ezz, 1984, Int. Metals Rev., 29, p136

M.V. Pridantsev, 1967, Izv. Acad. Nauk. SSSR Met., 5, p115

C.M.F. Rae, 1984, to be published

C.M.F. Rae and G.S. Hillier, 1984, to be published

I.L.F. Ray and D.J.H. Cockayne, 1970, Phil. Mag. 22, p853

I.L.F. Ray and D.J.H. Cockayne, 1971, Proc. Roy. Soc., A325, p543

I.L.F. Ray, R.C. Crawford and D.J.H. Cockayne, 1970, Phil. Mag., 21, p1027

D. Raynor and J.M. Silcock, 1970, Met. Sci. J., 4, p121

W.T. Read, 1953, Dislocations in Crystals, McGraw-Hill, New York, p207

J.E. Restall, The Development of Gas Turbine Materials, 1981, ed. G.W. Meetham, App. Sci. Publ., London, p259

R.A. Ricks, A.J. Porter and R.C. Ecob, 1983, Acta Met., 31, p42

Rolls-Royce Ltd., 1973, The Jet Engine, T.S.D. 1302

R.G. Roome, 1982, Report MEG 0645, Rolls-Royce Ltd., Derby

A.W. Ruff, 1970, Met. Trans., 2, p2391

P.L. Ryder and W. Pitsch, 1968, Phil. Mag., 18, 807

S.M.L. Sastry and B. Ramaswami, 1976, Phil. Mag. A, 33, p375

P.G. Self, M.P. Shaw and W.M. Stobbs, 1982, Phys. Stat. Sol. (a), 73, p.37

J.M. Silcock and W.J. Tunstall, 1964, Phil. Mag., 10, p361

A.E. Staton-Bevan and R.D. Rawlings, 1975a, Phil. Mag., A, 32, p787

A.E. Staton-Bevan and R.D. Rawlings, 1975b, Phys. Stat. Sol. (a), 29, p613

W.M. Stobbs, 1973, 3rd Course on Electron Microscopy in Materials Science, Erice, ECSC, Luxembourg, p591

W.M. Stobbs and C.H. Sworn, 1971, Phil. Mag., 24, p1365

H. Suzuki, 1952, Sci. Repts. Tohoku Univ., Japan, A4, p455

K. Suzuki, M. Ichihara and S. Takeuchi, 1979, Acta Met., 27, p193

R.J. Taunt, 1973, Ph.D thesis, Univ. of Cambridge

R.J. Taunt and B. Ralph, 1974, Phil. Mag., 30, p1379

S. Takeuchi and E. Kuramoto, 1973, Acta Met., 21, p415

S. Takeuchi, E. Kuramoto, T. Yamamoto and T. Taaka, 1973, Jap. J. Appl. Phys., 12, p1486

A. Taylor and R.W. Floyd, 1952, J. Inst. Metals, 81, p25

A.S. Tetelman, 1962, Acta Met., 10, p813

N. Thompson, 1951, Proc. Phys. Soc., 40, p1014

R.H. Thornton, R.G. Davies and T.L. Johnston, 1970, Met. Trans., 1, p207

J.K. Tien, B.H. Kear and G.R. Leverant, 1972, Scripta Met., p135

F.L. VerSnyder and R.W. Guard, 1960, Trans. ASM, 52, p485

F.L. VerSnyder and M.E. Shank, 1970, Mat. Sci. Eng., 6, p213

A.E. Vidoz and L.M. Brown, 1962, Phil. Mag., 7, p1167

J.M. Walsh and M.J. Donachie, 1969, Mat. Sci. J., 3, p68

C. Wells, 1981, The Development of Gas Turbine Materials, ed. G.W. Meetham, Appl. Sci. Publ., London, p207

M.J. Whelan, 1959, Proc. Roy. Soc., A219, p114

M.J. Whelan and P.B. Hirsch, 1957a, Phil. Mag., 2, p1121

M.J. Whelan and P.B. Hirsch, 1957b, ibid., 2, p1301

F. Whittle, 1930, U.K. Patent no. 347,206

M. Yamaguchi, V. Paidar, D.P. Pope and V. Vitek, 1982, Phil. Mag. A, 45, p867

M. Yamaguchi, V. Vitek and D.P. Pope, 1981, Phil. Mag. A, 43, p1027